Estimation of Transmission Line Parameters for Digital Equalization of High-Speed Data Radio

Benoît Pelletier

Department of Electrical & Computer Engineering
McGill University
Montréal, Canada

March 2002

A thesis submitted to the Faculty of Graduate Studies and Research in partial fulfillment of the requirements for the degree of Master of Engineering.

Abstract

This work considers the distortion created by an unmatched transmission line system at the receiver of a military data radio. The installation requirements for these types of systems are such that manual tuning of the antenna is impracticable. The antenna impedance may not match that of the cable and radio receiver, resulting in electrical reflections in the cable. These reflections create intersymbol interference (ISI), which distorts the received signal and limits the performance of the communication link.

It is shown that this distortion can be modelled using only four parameters: the transit time, the amplitude and the angle of the reflection coefficient and the synchronization offset. A joint maximum likelihood (ML) block estimator for the parameters is presented with the corresponding Cramér-Rao bound. The performance of the estimator is evaluated using simulations and compared to the bound. A more practical iterative estimator algorithm for the joint estimation of the parameters is also suggested.

To compensate for the distortion at the receiver, a filter design technique based on the estimated parameters is introduced. The method, obtained from the least squares procedure, produces an approximate inverse filter for the channel, minimizing the distortion at the receiver. Results comparing the proposed method to traditional adaptive equalizers are presented. They show that the minimum mean squared error (MSE) achieved by the proposed method approaches the power of the noise, the minimum value attainable.

Sommaire

Ce mémoire examine les effets de la distorsion créée par une mauvaise adaptation de l'impédance d'une antenne connectée par un câble à un récepteur radio de type militaire. L'ajustement manuel de l'antenne est impraticable dû aux exigences d'installation. Ainsi, l'impédance de l'antenne n'est pas nécessairement adaptée à celle du câble et du récepteur radio, résultant en des réflexions électriques dans le câble. Ces réflexions créent du brouillage intersymbole qui limite la performance du lien radio.

Il est démontré que cette distorsion peut être décrite entièrement avec l'utilisation de quatre paramètres: le temps de propagation, l'amplitude et l'angle du coefficient de réflexion et le délai de synchronisation. Un estimateur commun à maximum de vraisemblance (ML) en bloc est présenté avec la borne de Cramér-Rao (CRB) correspondante. La variance de l'estimateur ML est évaluée par simulations et les résultats sont comparés à la borne. Un algorithme d'estimateur itératif plus pratique est également suggéré.

Afin de réduire les effets de la distorsion au récepteur, une méthode de synthèse de filtre de compensation utilisant les paramètres estimés est présentée. Le filtre de compensation créé est une approximation de l'inverse du canal (entre l'antenne et le récepteur), qui permet de minimiser la distorsion au récepteur. Les résultats comparent le système de compensation proposé avec certaines autres techniques d'égalisation de canal plus traditionnelles. Ils démontrent que l'écart quadratique moyen obtenu avec la méthode proposée approche la puissance du bruit, valeur minimum à atteindre.

Acknowledgments

The completion of this thesis would not have been possible without the advice, guidance and expertise of my supervisor, Prof. Benoît Champagne. I would like to thank CMC Electronics Inc., formerly BAE SYSTEMS Canada Inc., and the Natural Sciences and Engineering Research Council of Canada (NSERC) for providing the financial support to carry this research as part of an Industrial Postgraduate Scholarship (IPS). I am also thankful for CMC Electronics Inc. that provided such a challenging project and Mr. Peter Perodeau for his help during the early stage of this research.

I am grateful to my fellow graduate students, Mark, François, Tarun, Chris, Wesley, Joachim, Xiaojian, Dorothy and Aziz, in the Telecommunications and Signal Processing Laboratory, for their companionship and for creating such an exciting work environment.

My gratitude goes to my friend Kim for her affection and understanding throughout my studies. I am forever indebted to my family for their love, support and encouragement throughout my life.

Contents

List of Figures

Chapter 1

Introduction

In this Chapter, the problem under consideration in this thesis is introduced, followed by a survey of the relevant literature. Then, the research objectives and methodology are exposed, the contributions are listed and finally, an outline of the thesis organization is given.

1.1 Problem Overview

In this work, a very specific radio unit designed for military communications is considered. This radio system provides a capacity of up to 8Mbps over 40km links, with a reliability better than 10^{-8} residual bit error rates, compatible with ATM requirements. The radio unit's reliability combined with its ease of use and flexibility makes it a leader in today's military communication systems.

The radio unit of interest is used by the military for general data traffic like digital speech, video and computer data transmission. The radio unit is usually located in a military communication truck, from which it is deployed. In a conflict situation, the location of the communication vehicle may change on a daily basis. For these reasons, the military requires that the radio link be installed in less that half an hour with the help of only three people. The work involved in setting the radio system is minimized; it consists of mounting the antenna on top of an elevated structure, connecting the cable between the antenna and radio, and selecting the radio operating frequency and related parameters.

The general data transmission problem consists of sending information through a channel and recovering the original data (see Fig 1.1). The digital information may originate from a variety of sources such as digital speech, computer file, digital video etc. The channel usually distorts

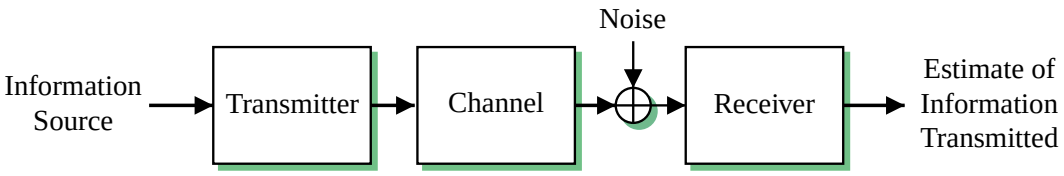

Fig. 1.1 General Data Transmission System

the transmitted signal and then noise is added to it. For this reason, the receiver, in general, cannot perfectly recover the transmitted data. This imperfection may cause errors in the decoded information which may have dramatic consequences in certain applications.

This work focuses on the distortion caused by the possible impedance mismatch of the antenna-cable-radio connection in the previously described radio system. Normal installation of a fixed wireless communication system involves tuning of the antenna-cable-radio connection. If the impedance of the antenna is not matched to that of the cable and radio receiver, there will be electrical reflections in the cable, as illustrated in Fig. 1.2. Therefore, in most commercial systems, the antenna is usually tuned manually as part of the installation process to minimize those reflections. However, manual adjustments of the antenna is impractical in the particular applica-

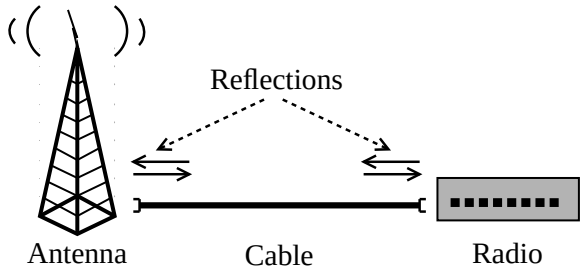

Fig. 1.2 Reflections from Impedance Mismatch

tion under study because it would most certainly violate the requirements of a limited installation time. Therefore, reflections in the antenna cable are bound to occur. These reflections will create distortion at the receiver.

Indeed, because the radio operates at a very high data rate (up to 2×10^6 symbols/second) and because the time delay between the incoming wave and its associated reflections is short due to the limited length of the cable, significant distortion or intersymbol interference (ISI) will be present at the receiver. Unfortunately, it is not possible to design an antenna that would only

require tuning at the manufacture because the impedance of the antenna is highly dependent on the operating frequency, which is subject to frequent changes. Furthermore, this radio unit operates in two distinct bands, ranging from 225 to 400 MHz and 1.3 to 2.7 GHz for the first and second band respectively. The frequency range is so large that it is very difficult, if not impossible, to build an antenna that would have the same properties for the entire range in each band.

Consequently, the particular application of this wireless radio system is such that distortion of the received signal caused by impedance mismatch on the antenna-cable-radio connection is inevitable. The characteristics of this distortion depend on the length of the cable or transmission line, the frequency of operation, the antenna type, the receiver structure, the temperature, the cable type and other parameters. Not only this distortion is inevitable but also, since this radio normaly operates with large signal-to-noise ratio, it is the major source of performance degradation.

The problem under study therefore consists of designing a compensation filter or system that minimizes or eliminates this performance limitation. The radio demodulator already has the hardware necessary for digital filtering of the received signal. More specifically, the modem possesses a quadrature 8–tap finite impulse response (FIR) equalizer located after the matched filter. The FIR filters are used as part of a non-optimal proprietary equalization scheme for impedance mismatch. The new compensating filter should preferably be designed to utilize the hardware available.

It is shown in this thesis through mathematical analysis of the channel model that its properties can be fully described by a finite number of parameters: the reflection coefficient, the time delay between reflections and the synchronization offset. It is therefore proposed here to approach the problem from a parameter estimation perspective. The channel parameters are to be estimated from the received signal. Based on the estimates and knowledge of the channel structure, a compensation filter will be designed on-line and loaded into the equalizer already present in the radio receiver. The procedure is illustrated in Fig. 1.3.

1.2 Literature Survey

The problem introduced above is very specific; it is in fact so specific, that finding articles on this exact topic in the literature is very difficult. Similar problems can be found in other fields of engineering like the triple transit echo problem related to surface acoustic waves in semicon-

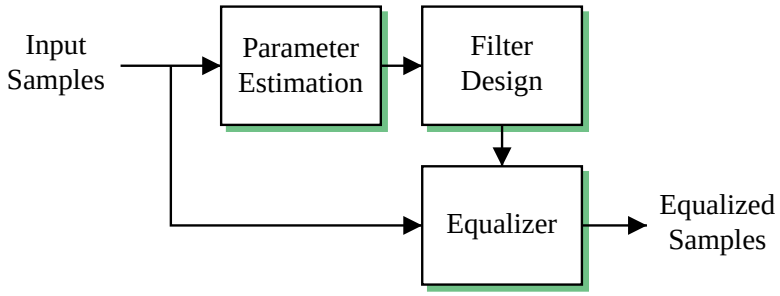

Fig. 1.3 Proposed Equalization Procedure

ductors [1, 2]. Although these problems are related, they belong to different fields of study in electrical engineering and have quite different solutions.

It could be said that the problem of interest here belongs to the class of general adaptive channel equalization. However, the structure of the channel is well known a-priori. This information should be used in the design of the compensation filter as opposed to the general problem, where no information about the channel is available. Thus, general adaptive channel equalization techniques will not take advantage of this information.

Nevertheless, some general adaptive equalization algorithms may be used to compensate for the distortion. Many adaptive filter algorithms have been applied to digital transmission. In particular, the *least mean square* or LMS algorithm can be applied to channel equalization [3] for QAM systems.

The LMS adaptive filter algorithm is often considered as the “standard” algorithm to which others algorithms are benchmarked to. Several algorithms based on LMS have been derived to achieve certain objectives like complexity reduction and better convergence. Example of these include the sign algorithm [4], the normalized LMS algorithm (NLMS), the affine projection algorithm (APA) and its fast version [5], the frequency-domain LMS algorithm, etc. Beside the LMS, another very popular adaptive filter algorithm is the recursive least square (RLS) algorithm and related modified algorithms such as the fast RLS (FRLS) and the frequency-domain approximate RLS algorithm [6].

More recently, a new category of blind adaptive filters designed specifically for data transmission has been developed. The *Constant Modulus Algorithm* (CMA) [7] has attracted much interest [8]. Its low complexity and convergence properties without the need for training (hence blind) are very attractive properties for high speed modems.

The approach that is proposed here involves the use of parameter estimation techniques. Estimation theory is a well-developed topic (e.g. see [9]), which originates from basic probability theory. One of the general objectives of parameter estimation is to obtain an estimate of a parameter, based on a set of many observations and a probability model. Estimation theory defines a mathematical base to obtain estimation functions from the probability model and to analyze the performance of the estimate. Standard procedures to obtain and analyze an estimator are straightforward and covered in many writings [9,10,11]. Additionally, the general procedure for this part of our work is based on relatively recent articles with similar objectives: [12, 13].

1.3 Objectives Approaches and Contributions

The main objective of this research is to incorporate channel information into the design of the equalizer or compensation filter and analyze its performance. In addition, the proposed method should be compared to other more general channel equalization techniques. The objective is then to determine if the proposed method is advantageous compared to general approaches.

The work may be divided in smaller parts so that specific objectives can be identified separately. This includes channel modelling, parameter estimation, compensation filter design and performance evaluation.

For the channel model, it is required to develop a complete accurate mathematical model for the distortion. The model must be accurate enough to closely represent the channel in the system and must be simple enough to be meaningful. Ideally, the channel should be parameterized so that its characteristics can be fully determined by a small set of parameters.

Then, an estimation procedure for the channel parameters needs to be developed and evaluated. It is desirable to have a estimator function that gives accurate estimates of the parameters because the estimates will be used to create a compensation filter for the channel. Bad estimates will inevitably result in a poor compensation filter. Therefore, the maximum likelihood (ML) estimator is developed along with the corresponding Cramér-Rao bound (CRB) on the estimator variance. The variance of the estimates obtained using the ML estimator will be measured through simulations and compared to the CRB.

The compensation filter needs to be designed such that the channel distortion effects are minimized or eliminated. Since the filter is limited in length to a small number of coefficients in the present application, it will be necessary to use a filter design technique that approximates the desired frequency response of the filter. The design method must be simple enough so that it can

be performed on-line.

Finally, it is required to evaluate the performance of this compensation system. The evaluation will be performed through a comparison with other channel equalization techniques such as the aforementioned NLMS. The evaluation should be performed over a large number of different channels and operating conditions to obtain a realistic measure of performance.

To achieve the objectives, the problem will first be analyzed mathematically. Then, simulations will be performed throughout the work to validate the theoretical findings. The numerical analysis computer tool *MATLAB* and the programming language C will be used.

The results obtained in this thesis show that it is possible to derive a reliable set of parameter estimates and design a compensation filter to equalize the channel distortion. The proposed compensation system is shown to perform better than some suboptimal adaptive channel equalizers.

As such, the contributions of this work to the body of research in the telecommunications and signal processing areas can be summarized as follow. First, the ML estimator for the unmatched transmission line system parameters, i.e. the reflection coefficient, the time-delay between reflections and the synchronization offset is derived. Then, a more practical ML iterative estimator is developed. The Cramér-Rao bound for the ML estimator is derived and finally, a compensation filter design technique that utilizes the estimated parameters for the equalization of the unmatched system is described.

1.4 Thesis Organization

A detailed description of the problem is presented in Chapter 2. Basic transmission line theory is introduced to assist the modelling of the reflections in the cable. Mathematical models for the channel and the communication system are developed. The communication system under study is detailed and simplified to an equivalent lowpass model. The statistics of the received symbols are discussed.

The concepts of parameter estimation are then introduced in Chapter 3. A parameter estimation technique for the channel parameters is developed and analyzed. The probability model for the parameters based on the received samples is derived. Practical considerations are discussed including a proposed iterative implementation of the ML estimation procedure. The block joint ML estimator is also discussed and the Cramér-Rao lower bound is derived.

Compensation filter design is discussed in Chapter 4, which begins with a discussion of the ideal channel equalizer. Design issues are then discussed, in particular the implementation of

fractional delays in discrete-time systems is considered. The procedure to obtain the coefficients of the compensation filter is then examined.

The results comparing the standard channel equalization techniques to the proposed algorithm solution are presented in Chapter 5 as well as some results on the parameter estimation procedure. Finally, Chapter 6 summarizes and concludes this work.

Chapter 2

Background and Problem Definition

In this Chapter, necessary background material is introduced along with a definition of the specific problem under consideration. The chapter starts with a brief introduction to transmission line theory. This is followed by a description of the channel under consideration and its properties. Then, the communication model that will be used throughout this work is studied. Finally, the problem of interest in this thesis is defined in formal terms.

2.1 Introduction to Transmission Line Theory

In Chapter 1, the source of the distortion at the receiver is introduced as an impedance mismatch in the receiver-cable-antenna system (see Fig. 1.2). To model and analyze this source of distortion, understanding electric transmission line properties, and more specifically reflections, is essential.

An electric transmission line is a passive physical device, consisting of two parallel conductors, that carries an electromagnetic signal from one end to the other, usually attenuating its amplitude and modifying its phase. Not all pairs of parallel conductors are transmission lines; conductors that are much smaller in length than the shortest wavelength of the signal they carry are not considered transmission lines.

Since the signals propagating over transmission lines are often modulated, as is the case here, at some carrier frequency, say ω_c, they are typically modelled using phasor to simplify the notation. Consider the semi-infinite transmission line illustrated in Fig. 2.1. Using phasor notation, the voltage $v(z,t)$, referenced to cosine, measured at location z and time t on the semi-

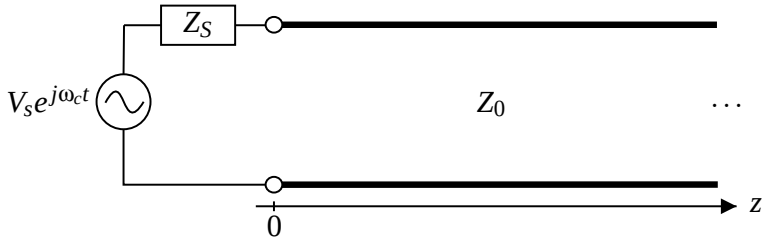

Fig. 2.1 Semi-infinite Transmission Line

infinite transmission line is expressed as

$$v(z,t) = \text{Re}[V(z)e^{j\omega_c t}], \tag{2.1}$$

where $V(z)$ is the voltage at distance z on the line, now independent of time. This representation allows us to make abstraction of the carrier in the time domain.

The properties of a transmission line are modelled using only a few parameters, which have an implicit dependence on the carrier frequency ω_c. The propagation constant, denoted by γ, determines how the transmission line attenuates and changes the phase of a sinusoidal wave with distance:

$$\gamma = \alpha + j\beta, \tag{2.2}$$

where α is the *attenuation constant* (Np[1]/m), which characterizes attenuation per meter, and β is the *phase constant* (rad/m), a measure of phase shift per meter [14]. Specifically, if a source voltage V_S is applied at the input of a semi-infinite transmission line, the voltage on the line at distance z from the source becomes:

$$V(z) = V_S e^{-\gamma z}. \tag{2.3}$$

The ratio of voltage to current at any point on a transmission line is called the *characteristic impedance* and is denoted by Z_0:

$$Z_0 = \frac{V(z)}{I(z)}. \tag{2.4}$$

Note that it is called "characteristic" because for a semi-infinite transmission line (with no reflec-

[1] An attenuation of 1 Neper (Np) applied to a wave corresponds to its amplitude being decreased to $e^{-1} \approx 0.368$ of its original value.

tions), this ratio is constant and consequently independent of z. Also, note that Z_0 and γ both characterize the physics of the transmission line structure as they are independent of the position on the line.

For a semi-infinite transmission line, it is true that the ratio of voltage to current is constant and equals the characteristic impedance. However, when the transmission line is terminated by some load, it is not generally the case anymore. Specifically, when a transmission line is terminated by a load impedance (Z_L) different from the characteristic impedance of that line (Z_0), a *reflection* occurs. Two travelling waves then exist on the line; an incident wave, going from the source to the load and a reflected wave, going from the load back to the source.

The ratio of reflected to incident voltage wave is given in phasor notation by the *voltage reflection coefficient* [14]:

$$\Gamma_L = \frac{Z_L - Z_0}{Z_L + Z_0} = |\Gamma_L| e^{j\theta_\Gamma}. \tag{2.5}$$

In general, Γ_L is complex and $|\Gamma_L| < 1$. From (2.5), it is obvious that if the impedances match (i.e. $Z_L = Z_0$), Γ_L is zero and no reflection occurs.

Figure 2.2 illustrates a simple transmission line system with finite length L_c, characteristic impedance Z_0, voltage source V_S, source impedance Z_S and load impedance Z_L. If the source

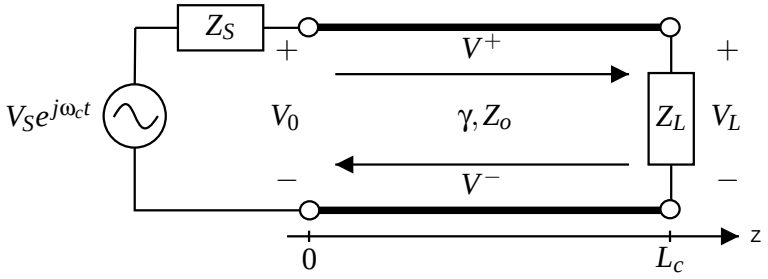

Fig. 2.2 Transmission Line Model

and load impedances are not assumed to be matched to the characteristic impedance of the transmission line, reflection occurs on both ends of the transmission line.

When the source is turned on, the voltage V_0 that first appears at the source end of the transmission line is given by simple voltage division:

$$V_0 = V_S \frac{Z_0}{Z_0 + Z_S}. \tag{2.6}$$

This voltage travels on the transmission line until it hits the load. Then, it gets reflected and two waves now coexist on the transmission line; a forward and backward travelling wave. The total voltage at any point is given by the sum of the two wave voltages.

Let $V^{n+}(z)$ and $V^{n-}(z)$ denote the n^{th} reflected forward (z increases with time) and backward (z decreases with time) travelling wave voltages respectively, measured at distance z from the source. $V^{0+}(z)$ becomes the first forward travelling incident wave voltage and $V^{0-}(z)$ the first backward travelling wave voltage. Let Γ_S represent the source reflection coefficient such that

$$\Gamma_S = \frac{Z_S - Z_0}{Z_S + Z_0}. \tag{2.7}$$

Then, from the discussion above and the definitions of Γ_L, Γ_S and V_0, $V^{n+}(z)$ and $V^{n-}(z)$ can be expressed as

$$V^{n+}(z) = V_0(\Gamma_L\Gamma_S)^n e^{-\gamma(2nL_c+z)} \tag{2.8}$$

$$V^{n-}(z) = V_0(\Gamma_L\Gamma_S)^n\Gamma_L e^{-\gamma(2n+1)L_c}e^{-\gamma(L_c-z)} \tag{2.9}$$

The voltage measured at the load in steady-state is given by the sum of the forward and backward travelling wave voltages at position $z = L_c$, summed over all reflections i.e:

$$V_L = \sum_{n=0}^{\infty}(1+\Gamma_L)V_0(\Gamma_L\Gamma_S)^n e^{-\gamma(2n+1)L_c}. \tag{2.10}$$

Using a well known property of the geometric series, this last equation simplifies to

$$V_L = V_0 e^{-\gamma L_c}\frac{1+\Gamma_L}{1-\Gamma_L\Gamma_S e^{-\gamma 2L_c}}, \tag{2.11}$$

which holds provided that $|\Gamma_L\Gamma_S e^{-\gamma 2L_c}| < 1$ which is always the case since $|\Gamma_L| < 1$, $|\Gamma_S| < 1$ and $|e^{-\gamma 2L_c}| = 1$ by definition.

2.2 Channel Description

In the previous section, the voltage relation between the source and the load for the particular transmission line system of Fig. 2.2 was developed. This system may be regarded as the one illustrated in Fig. 1.2. The source would corresponds to the antenna, the transmission line to the

physical cable and the load to the radio receiver. The antenna-cable-receiver connection is then considered as a channel that distorts the signal at the receiver. A mathematical description of this channel is required to devise a mechanism to recover the data more efficiently.

To obtain such description, it is first noted that the bandwidth used by radio transceiver is very small compared to the carrier frequency. In fact, the radio unit considered operates in two bands, from 225 to 400 MHz for the first band and 1.3 to 2.7 GHz for the second band, and has a transmission bandwidth of at most 5MHz at the maximum rate. Therefore, it is reasonable to assume that the frequency-dependent parameters are fixed for a small bandwidth around the carrier (e.g. see for example the specifications for a commercial microwave cable [15]).

Then, it is observed that the length of the line L_c may be expressed in terms of time delays. Let μ denote the wave propagation velocity in the transmission line. If τ denotes the time required for the wave to propagate from one end of the line to the other, i.e. a distance L_c, then

$$\tau = \frac{L_c}{\mu}. \tag{2.12}$$

Let us introduce the phase constant [14],

$$\beta = \frac{\omega}{\mu}, \tag{2.13}$$

where $\omega = 2\pi f$ is the wave angular frequency. Using (2.2), (2.12) and (2.13), the factor γL_c appearing in (2.11) can be expressed as follows

$$\gamma L_c = \alpha L_c + j\omega\tau. \tag{2.14}$$

With the help of (2.14), (2.11) may be written in the form of a frequency dependent transfer function as follows:

$$H(\omega) \triangleq \frac{V_L}{V_0} = e^{-\alpha L_c} e^{-j\omega\tau} \frac{1+\Gamma_L}{1-\Gamma_L\Gamma_S e^{-\alpha 2L_c} e^{-j\omega 2\tau}}. \tag{2.15}$$

Introducing the complex-valued constants

$$\psi = \Gamma_L\Gamma_S e^{-\alpha 2L_c} \tag{2.16}$$

$$\phi = e^{-\alpha L_c}(1+\Gamma_L), \tag{2.17}$$

then $H(\omega)$ may be expressed more compactly as

$$H(\omega) = \frac{\phi e^{-j\omega\tau}}{1 - \psi e^{-j\omega 2\tau}}, \tag{2.18}$$

where ψ and ϕ are assumed to be independent of ω in the carrier neighborhood. It can be observed from $H(\omega)$ that its magnitude response is periodic in frequency, with a period of $\Delta f = \frac{1}{2\tau} = \frac{\mu}{2L_c}$.

Example

Figure 2.3 shows the magnitude and phase responses for a hypothetical system, with cable length $L_c = 25$m, reflection coefficients $\Gamma_S = -6$dB and $\Gamma_L = -10$dB, attenuation $\alpha = -5$dB/m and wave propagation velocity $\mu = 2.5 \times 10^8$m/s (typical for the cable types used). The carrier frequency is 2GHz, corresponding to the middle of the second band and the system bandwidth is 5MHz. As seen in Figure 2.3 the frequency response $H(\omega)$ is periodic in ω with a period of

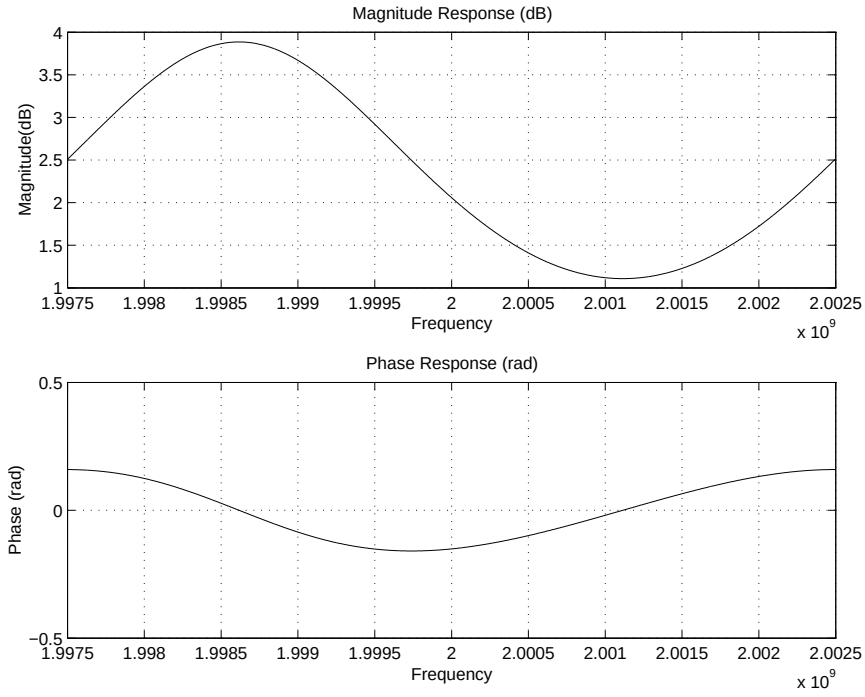

Fig. 2.3 Channel Frequency Response

5MHz, which is equal to $\frac{\mu}{2L_c}$.

Note that this is an over-simplified example; indeed the reflection coefficients were taken as real and positive while in practice, they can be anywhere inside the unit circle of the complex plane. The response can thus vary greatly from what is shown in Fig. 2.3. Nevertheless, it gives a good idea of the general shape of the channel's frequency response.

2.3 Communication System Model

In this section, the mathematical model for the communication system under investigation is developed and its baseband representation is discussed. To begin, the characteristics of the communication system are described and then the lowpass equivalent representation is derived.

2.3.1 Communication System Characteristics

The system under consideration[2] consists of a wireless radio system capable of transmitting at a rate up to 8Mb/s. It uses trellis-coded modulation (TCM) with 32 quadrature amplitude modulation (QAM) symbols. TCM is a coding technique [16] that is outside of the scope of this work and will not be considered. Figure 2.4 illustrates the system's block diagram. The different components present in the block diagram are described below, starting from the binary source up to the binary sink at the receiver output.

- Binary source: Source of binary digits to be transmitted. It is assumed that the two binary symbols have the same probability of occurrence. The bits are generated at a rate of 8Mb/s.

- MAP: This block groups binary digits together and maps them into a corresponding QAM symbol A_k, with k denoting a time index. This symbol is composed of "real" and "imaginary" parts corresponding to the in-phase (top) and quadrature (bottom) branches in the block diagram. The symbols are forwarded to the pulse shaping function periodically, every $T = 0.5 \times 10^{-6}$ second. Notice that an extra bit is added for the TCM, which is not considered in this work. The output symbol rate is therefore 2×10^6 symbols per second or 2Ms/s.

- $p(t)$: The pulse shaping function. It has the spectrum characteristics of the square root of a

[2]The following description of the radio system was obtained from: P. Perodeau, Private Communication, CMC Electronics Inc., July 2000.

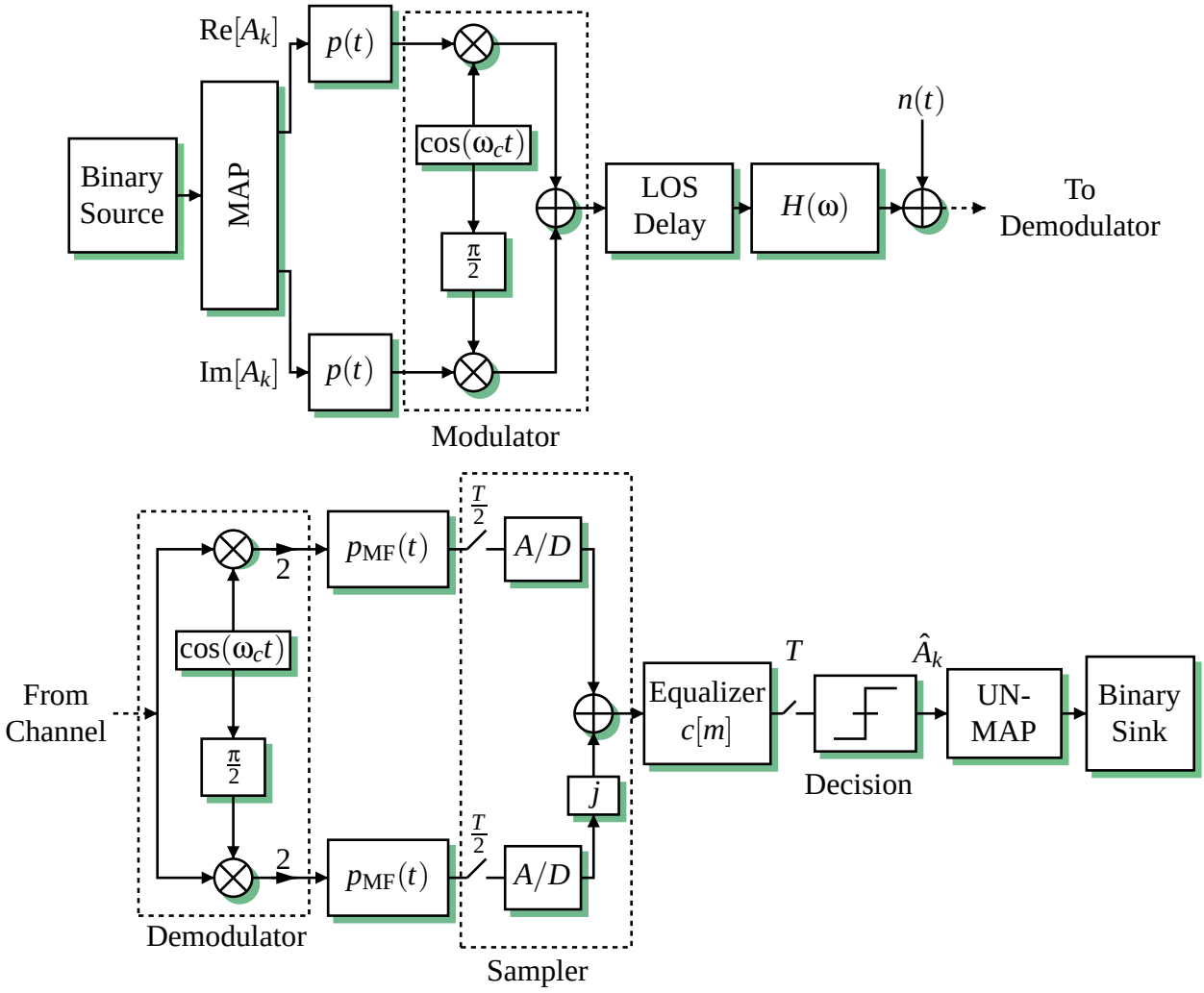

Fig. 2.4 Complete Communication System Model

raised cosine. Thus, $P(\omega) = \sqrt{G(\omega)}$, where $G(\omega)$ is given by

$$G(\omega) = \begin{cases} T, & |\omega| < \frac{1-\beta}{T}\pi \\ \frac{T}{2}\left\{1 + \cos(\frac{T}{2\beta}(|\omega| - \frac{1-\beta}{T}\pi))\right\}, & \frac{1-\beta}{T}\pi \leq |\omega| \leq \frac{1+\beta}{T}\pi \\ 0, & |\omega| > \frac{1+\beta}{T}\pi, \end{cases} \tag{2.19}$$

where β is called the *rolloff* factor, $0 \leq \beta \leq 1$ and T is the symbol period, defined above. In the time-domain, the expressions for $p(t)$ and $g(t)$ are given respectively by

$$p(t) = \frac{(4\beta t/T)\cos(\pi(1+\beta)t/T) + \sin(\pi(1-\beta)t/T)}{(\pi t/T)[1-(4\beta t/T)^2]}, \tag{2.20}$$

$$g(t) = \text{sinc}(\frac{\pi t}{T})\frac{\cos(\frac{\pi\beta t}{T})}{1 - \frac{4\beta^2 t^2}{T^2}}. \tag{2.21}$$

It can be noted from (2.19) that the raised cosine frequency response is limited to $|\omega| < W$, where W is the system's bandwidth[3] defined as

$$W = \frac{(1+\beta)\pi}{T}. \tag{2.22}$$

Notice that according to the given definition of bandwidth, the modulated (bandpass) raised cosine has bandwidth $2W$.

- Modulation: The following step consists of modulating the signal. The in-phase component (top branch) is modulated at frequency ω_c directly via multiplication with $\cos(\omega_c t)$. The quadrature component (bottom branch) is also modulated at ω_c but is phase shifted by $-\pi/2$ with respect to the in-phase component. The two signals are then added together (no information is lost since the two signals are in phase-quadrature).

- Line-of-sight (LOS) Delay: This is the physical channel between the two antennas. Since a line-of-sight (LOS) is assumed with no multipath components, it consists of a pure delay, with no distortion. This assumption holds in the present context where the installation procedure requires that the antenna be installed in such a way as to minimize the multipath

[3] In this thesis, the bandwidth is defined as the extent of significant spectral content of the signal for positive frequencies [17].

reflections (e.g. the antenna is placed behind a blocking structure like a truck or small building in such a way as to prevent as much multipath components as possible from reaching the antenna while leaving the direct path unaffected).

- $H(\omega)$: The channel impulse response created by reflections in the antenna-cable-radio connection. The corresponding frequency response is defined in (2.18).

- $n(t)$: Narrowband noise, centered around the carrier frequency ω_c with bandwidth $2W = \frac{2(1+\beta)\pi}{T}$ and flat power spectral density (PSD) of amplitude $N_o/2$ (see section 2.4).

- Demodulation: Coherent demodulation with perfect phase synchronization is assumed. In practice, a *phase locked loop* is in place to ensure carrier tracking. The demodulation step separates the signal from the cable back into its in-phase (top) and quadrature (bottom) components. The factors of 2 normalize the input signal so that the quadrature components are scaled correctly. In practice, this is implemented using *automatic gain controllers* (AGC).

- $p_{\text{MF}}(t)$: These blocks represents the matched filters, selected to ensure a maximum peak signal-to-noise ratio (SNR) at the receiver.

- Sampler: Sampling and analog to digital conversion (A/D) allow the signal to be processed numerically. The analog signals are sampled at twice the baud rate i.e. $T/2$, synchronized with the middle of the symbol and then converted to a digital form. In this work, the following assumptions are made:

  i. the synchronization is not perfect and creates a time offset in the received signal, denoted by ϵ. This synchronization offset is to be incorporated in the channel model as a pure delay.

  ii. the A/D devices have high numerical precision, although in practice, the A/D converters would be limited to a fixed number of bits, depending on the implementation.

  iii. there is no aliasing caused by the sampling operation. Since the system's bandwidth is limited to the raised cosine bandwidth, it can be easily shown that a sampling rate of twice the baud rate guarantees no aliasing.

After the A/D conversion, the top and bottom branches are merged into a single complex entity, the in-phase and quadrature component corresponding respectively to its real and imaginary part.

- Equalizer ($c[m]$): this is the filter that compensates for the distortion caused by the channel $H(\omega)$. At the equalizer output, the signal is sampled at the baud rate, i.e. $1/T$.
- Decision device: this device decides which symbol was the most probably sent, given what has been received (using a shortest distance algorithm). The result is an approximation to the symbol sent which is denoted by $\hat{A}_k$.
- Symbol un-map: this device un-maps the symbol received into a sequence of binary digits.
- Binary Sink: this is the binary information's final destination.

2.3.2 Equivalent Lowpass Representation

Most communication systems use some sort of modulation to transfer information through a bandlimited channel. When the channel bandwidth is much smaller than the modulation carrier frequency, the system is said to be a narrowband bandpass system. The same definition applies to signals and in general, narrowband bandpass signals and systems can be represented by a lowpass equivalent form, which allows abstraction of the carrier modulation. Indeed, this form is more convenient and efficient to manipulate.

To obtain the lowpass equivalent of a narrowband bandpass signal, the pre-envelope must be computed, followed by its complex envelope (another name for lowpass equivalent). The procedure is illustrated in Fig. 2.5 and is explained below.

Consider a real narrowband bandpass signal $s(t)$, with frequency content concentrated in a finite window around a center frequency ω_c, as shown in Fig. 2.5(a). The pre-envelope of $s_+(t)$ is defined as

$$s_+(t) = s(t) + j\hat{s}(t) \tag{2.23}$$

where $\hat{s}(t)$ is the Hilbert transform [17] of $s(t)$. The pre-envelope consists of the original positive frequency signal spectrum scaled by two with its negative frequencies eliminated as illustrated in Fig. 2.5(b). The complex envelope $\tilde{s}(t)$ of $s(t)$ is given by

$$\tilde{s}(t) = s_+(t)e^{-j\omega_c t} \tag{2.24}$$

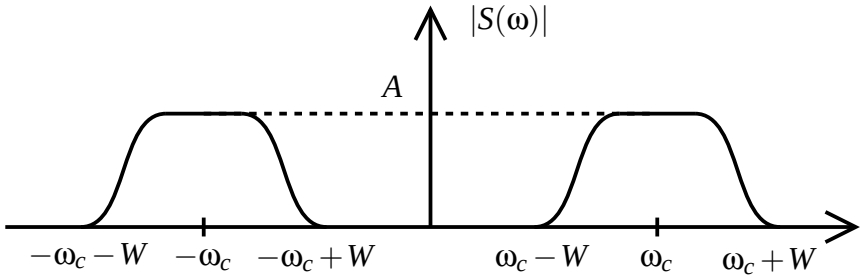

(a) Bandpass Signal

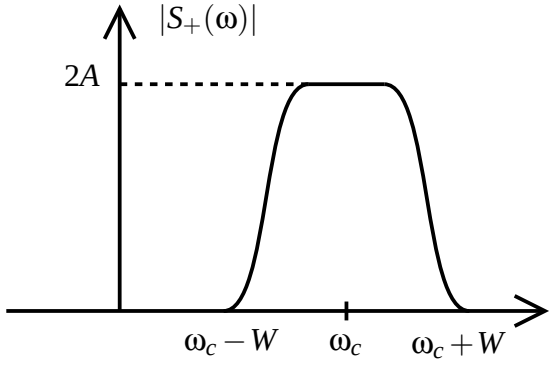

(b) Pre-envelope

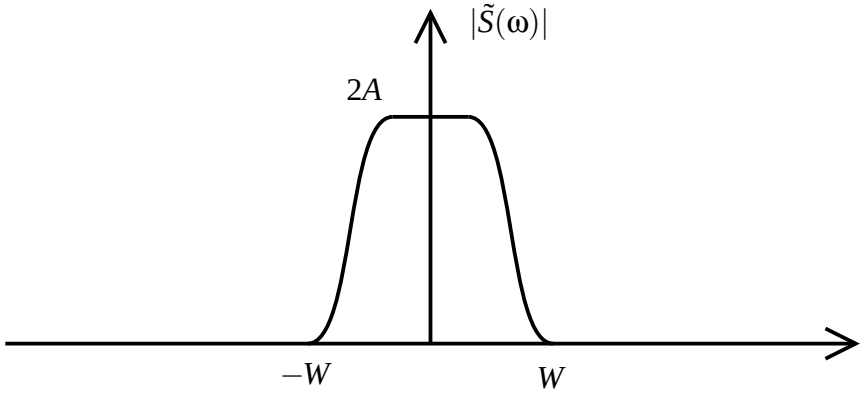

(c) Complex Envelope

Fig. 2.5 Lowpass Equivalent

and consists of a translation of the pre-envelope spectrum to baseband, as illustrated in Fig. 2.5(c). In general, $\tilde{s}(t)$ is complex valued and it can be expressed as:

$$\tilde{s}(t) = s_I(t) + j s_Q(t), \tag{2.25}$$

where $s_I(t)$ and $s_Q(t)$ are the so-called in-phase and quadrature components, respectively. The original bandpass signal can be recovered from its complex envelope using

$$s(t) = \text{Re}\left[\tilde{s}(t)e^{j\omega_c t}\right] \tag{2.26}$$

or equivalently from the in-phase and quadrature components:

$$s(t) = s_I(t)\cos(\omega_c t) - s_Q(t)\sin(\omega_c t). \tag{2.27}$$

Bandpass systems can also be represented in lowpass equivalent form using a similar procedure [17]. It can be shown that when a narrowband bandpass signal $s(t)$ passes through a bandpass system $h(t)$, the equivalent lowpass response of the output, say $\tilde{y}(t)$, is obtained using a normalized convolution (i.e. scaled by $1/2$):

$$\tilde{y}(t) = \frac{1}{2}\int_{-\infty}^{\infty} \tilde{s}(\tau)\tilde{h}(t-\tau)d\tau \tag{2.28}$$

$$= \frac{1}{2}(\tilde{s} * \tilde{h})(t) \tag{2.29}$$

2.3.3 Communication System Lowpass Equivalent

A complete lowpass equivalent for the communication system illustrated in Fig. 2.4 can be developed, using the concepts introduced in the previous section which allow abstraction of the modulation. Figure 2.6 illustrates the resulting lowpass equivalent communication system model, which consists of the following blocks, from the source to the sink: serial binary source (input), complex symbol mapping, pulse shaping filter, channel, noise source, matched filter, half symbol sampler, equalizer, symbol sampler, non-linear decision device, symbol to binary mapping, binary sink (output). The details of the derivation of the low-pass equivalent model are discussed in Appendix A. Only the essential equations and concepts are discussed below.

The output of the complex symbol mapping block is modelled as a sequence of complex numbers $A_k (k \in \mathbb{Z})$, where k denotes the discrete time index. It is convenient to express symbol

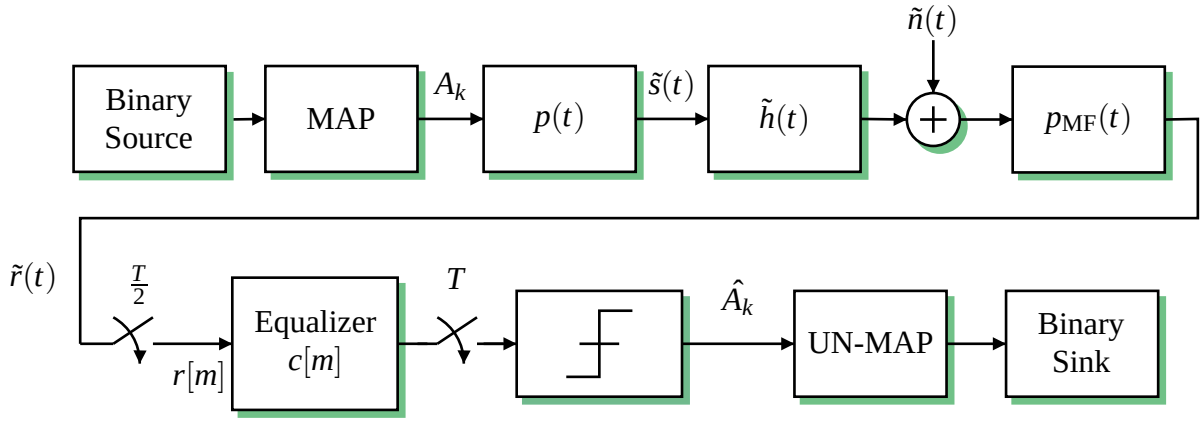

Fig. 2.6 System Model

A_k in term of its real and imaginary parts as

$$A_k = A_{Ik} + jA_{Qk} \tag{2.30}$$

The symbols A_k are chosen from a finite alphabet. The set of values they can assume depends on the *constellation* being used. The constellation for a particular system is obtained by plotting all the possible symbols complex amplitudes on the complex plane. The radio system of interest uses the QAM-32 constellation illustrated in Fig. 2.7. The lowpass equivalent transmitted signal, $\tilde{s}(t)$, consists therefore of a sum of pulsed shaped symbols:

$$\tilde{s}(t) = \sum_{k=-\infty}^{\infty} A_k p(t - kT) \tag{2.31}$$

where T is the symbol duration and $p(t)$ is the pulse shaping function. The received signal $\tilde{r}(t)$ at the sampler input may therefore be expressed as

$$\tilde{r}(t) = \frac{1}{2}(\tilde{s} * \tilde{h} * p_{\mathrm{MF}})(t) + (\tilde{n} * p_{\mathrm{MF}})(t), \tag{2.32}$$

where $\tilde{h}(t)$ is the channel impulse response, $\tilde{n}(t)$ is the noise term, $p_{\mathrm{MF}}(t)$ is the matched filter, i.e. a filter with impulse response $p(T-t)$, and "$*$" denotes convolution. The factor $\frac{1}{2}$ comes from the convolution of the two lowpass equivalent signals $\tilde{s}(t)$ and $\tilde{h}(t)$ (see eq. (2.28). It is shown in

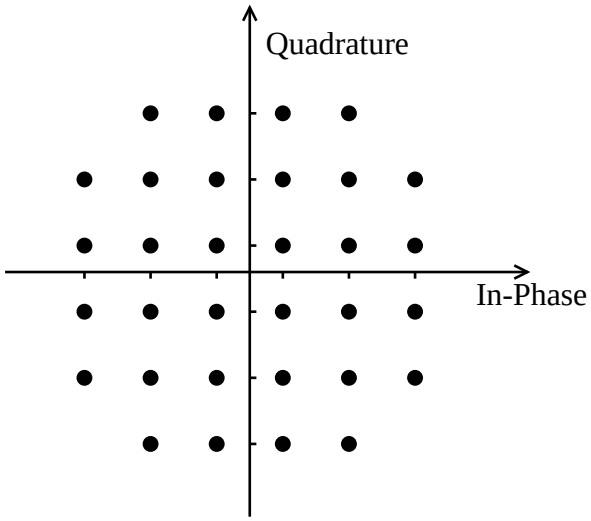

Fig. 2.7 QAM-32 Constellation

Appendix A that the received signal after matched filter may be expressed as

$$\tilde{r}(t) = \sum_{k=-\infty}^{\infty} \sum_{l=0}^{\infty} \psi^l A_k g(t - kT - 2l\tau) + v(t), \tag{2.33}$$

where $g(t)$ is given in (2.21) and $v(t)$ is defined by

$$v(t) = (\tilde{n} * p_{\text{MF}})(t) = \int_{-\infty}^{\infty} \tilde{n}(\xi) p_{\text{MF}}(t - \xi) d\xi. \tag{2.34}$$

Before equalization, the received signal is sampled at twice the baud rate. The symbol synchronization is not perfect due to the signal distortion. Hence, a synchronization offset ϵ is included in the model. Thus, after sampling at twice the baud rate, the discrete-time received signal is

$$r[m] = \sum_{k=-\infty}^{\infty} \sum_{l=0}^{\infty} \psi^l A_k g(m\frac{T}{2} - kT - 2l\tau - \epsilon) + v[m], \tag{2.35}$$

where the noise term $v[m]$ is given by

$$v[m] = v(\frac{mT}{2} - \epsilon) \tag{2.36}$$

and $m \in \mathbb{Z}$ represents the discrete time index. The synchronization offset ϵ has no effects on the noise because it is assumed stationary (see next section).

2.4 Statistical Properties

In this section, the statistical properties of the transmitted symbols and of the noise are discussed.

The symbols transmitted are selected from a discrete set of values, determined by the constellation. The sequence of A_k represents the realization of a random process, consisting of a sequence of independent and identically distributed (iid) random variables. The individual random variables have zero mean and are assumed to be uniformly distributed over the set of points defined by the constellation (see Fig 2.7). It is further assumed that the random process is *ergodic* in the mean and in the autocorrelation so that its statistical properties can be approximated from a finite set of observations [18], i.e.

$$\lim_{K\to\infty} \frac{1}{K} \sum_{k=0}^{K-1} A_k = E[A_k] = 0 \tag{2.37a}$$

$$\lim_{K\to\infty} \frac{1}{K} \sum_{k=0}^{K-1} A_k A_{k+l}^* = E[A_k A_{k+l}^*] = P_{\mathrm{A}}\delta[l], \tag{2.37b}$$

where P_{A} represents the average power of the constellation, A_k^* the complex conjugate of A_k and

$$\delta[l] = \begin{cases} 1, & l = 0 \\ 0, & \text{otherwise.} \end{cases} \tag{2.38}$$

The non-linear detector at the receiver makes decision on the received symbols and selects the symbol from the set that is the closest to the corresponding received sample. The radio system considered in this work has a very low probability of bit error ($\approx 10^{-8}$), which is partly due to trellis-coded modulation (TCM).

In this thesis, the symbols A_k shall be assumed to be detected without error. This assumption allows to focus on the parameter estimation and ignore the symbol detection problem. Therefore, A_k will represent a deterministic sequence, to which the ergodic properties in (2.37a) and (2.37b) apply. The effects of detection error in A_k will be considered in Chapter 5.

The noise $n(t)$ at the input of the receiver in Fig. 2.4 is assumed to be zero mean, narrowband

Gaussian with flat power spectral density of amplitude $N_o/2$ (bandpass white noise):

$$S_n(\omega) = \begin{cases} \frac{N_o}{2}, & \omega_c - W \leq |\omega| \leq \omega_c + W \\ 0, & \text{otherwise}, \end{cases} \tag{2.39}$$

where $2W$ represents the bandpass system bandwidth. It can be shown [17] that the lowpass equivalent noise is stationary and has mean and power spectral density

$$E[\tilde{n}(t)] = 0 \tag{2.40}$$

$$S_{\tilde{n}}(\omega) = \begin{cases} N_o, & |\omega| < W \\ 0, & \text{elsewhere}. \end{cases} \tag{2.41}$$

Since $S_n(\omega)$ is symmetric about ω_c, the in-phase and quadrature components of $\tilde{n}(t)$ are statistically independent [17]. Note that $\tilde{n}(t)$ is a complex circular Gaussian process as described in [19].

The correlated noise term $v(t)$ at the output of the matched filter, as given by eq. (2.34), is therefore also zero-mean complex circular Gaussian. Since the magnitude squared of the pulse shape frequency response $P(\omega)$ is exactly the raised cosine frequency response given in (2.19), the power spectral density of $v(t)$ is therefore

$$S_v(\omega) = N_o G(\omega). \tag{2.42}$$

with autocorrelation function

$$R_v(t) = N_o g(t). \tag{2.43}$$

Finally, the autocorrelation function for the sampled noise term $v[m]$ is given by

$$R_v[q] = E[v[m]v^*[m+q]] = N_o g(\frac{qT}{2}), \quad q \in \mathbb{Z}. \tag{2.44}$$

2.5 Research Problem

The received signal at the input of the equalizer contains information not only on the transmitted symbols, but also on the channel properties. In fact, observing the expression for $r[m]$ in (2.35), it can be seen that the channel parameters, ψ, τ and ϵ, are embedded in the equation.

The first part of the problem therefore consists of estimating the channel's parameters ψ, τ and ϵ, from a set of many observations, $r[m], m \in \{0, 1, \ldots, M\}$. Then, using those estimates, the second part of the problem is to design a discrete-time compensation filter for the channel.

In this thesis, the estimation problem is approached using statistical parameter estimation techniques. In particular, Chapter 3 discusses the maximum likelihood estimation technique, which is suitable to solve this problem. The difficulty is to find a simple estimator function that gives good, i.e. statistically reliable, estimates. The quality of the estimates will affect the compensation filter performance since it is designed using those parameter estimates.

The discrete-time compensation filter design is based on a least squares procedure. The difficulty in this problem is to have a good frequency response that cancels or reduces the intersymbol interference created by the channel, with a limited-length filter. The issues related to the filter design are discussed in details in Chapter 4.

Chapter 3

Maximum Likelihood Parameter Estimation

In this Chapter, the use of parameter estimation techniques for obtaining the characteristics of the channel described in Chapter 2 is discussed. The ultimate objective is to use the channel parameter estimates to create a compensating filter to reduce channel distortion. To begin, basic elements of parameter estimation theory are introduced. Then, the joint block maximum likelihood estimator for the channel parameters is developed. Practical considerations related to its implementation, including an iterative solution for the joint estimator are then discussed. Finally, the Cramér-Rao lower bound for the variance of the estimates is derived.

3.1 Parameter Estimation

Broadly stated, the parameter estimation problem consists of estimating the value of an unknown parameter θ, given a set of N observations or measurements represented by the vector

$$\boldsymbol{r} = [r[0], r[1], \ldots, r[N-1]]^T . \tag{3.1}$$

This is possible if given θ, a model for the probability density function (pdf) of the observation vector $\boldsymbol{r}$ is available.

Parameter estimation problems fall into two categories: *point estimation* and *Bayesian estimation*. In the case of point estimation, θ is not a random variable. The probability density function $p(\boldsymbol{r}; \theta)$ represents a *family* of pdf, specified by the parameter. The semi-colon ";" indi-

cates that the density is parameterized by θ. In point estimation, the parameter is estimated by choosing among the available family of pdf, the one that fits the "best" to the data. In the case of Bayesian estimation, θ is random and characterized by an *a-priori* probability density function $p_\theta(\theta)$ assumed to be known. The probability model for the received vector then becomes the conditional probability density function of $\boldsymbol{r}$ given the parameter θ, denoted $p_{\boldsymbol{r}|\theta}(\boldsymbol{r}|\theta)$, also assumed to be known. A Bayes estimate can be obtained as an estimate that minimizes the mean of a user-defined cost function [9]. Point estimation can be viewed as a special case of Bayesian estimation under the assumption of a uniform a-priori probability density function $p_\theta(\theta)$.

In this work, only non-random parameters are considered. Accordingly, the attention is focused to point estimation. Specifically, maximum likelihood (ML) estimation is examined next.

3.1.1 Maximum Likelihood Estimation

Maximum likelihood estimation may be used in cases where the parameter to be estimated is either non-random or has no known pdf. The following introduces basic theory of ML estimation. To begin, the concepts of bias and variance of an estimate are introduced. Then, the maximum likelihood estimator is defined for single and multiple parameters. Finally, the Cramér-Rao lower bound is presented.

Performance Measures

In order to evaluate and compare the properties of an estimate, its desirable characteristics must first be defined. In general, it is desired that the expected value of the parameter estimate be equal to the true value of the parameter and have small statistical variations of the estimate. Therefore, the objective performance measures are defined to be the estimate mean and variance.

Let $\hat{\theta}(\cdot)$ denote the *estimator* function and $\hat{\theta}(\boldsymbol{r})$ represent the estimate of θ at the observation point $\boldsymbol{r}$. The *bias* $B(\theta)$ of an estimate, as a function of the parameter, is then defined to be the difference between the expected value of the estimate and the true value of the parameter i.e:

$$B(\theta) \triangleq E[\hat{\theta}(\boldsymbol{r})] - \theta, \tag{3.2}$$

An estimate is said to be *unbiased* if $B(\theta) = 0$ for all values of θ of interest. Otherwise it is said to be *biased*. If a biased estimate gives a constant known bias independent of the parameter, then this bias can be subtracted from the estimate, and the latter becomes unbiased.

Even if an estimator gives unbiased estimates, it may still give a bad result on a single trial; it is only on average that the estimate is unbiased. To account for this possibility, the other performance metric, the estimate's variance, gives a measure of how much the estimate varies on average between trials. The variance of an unbiased estimate is given by:

$$Var[\hat{\theta}(\boldsymbol{r})] = E\{|\hat{\theta}(\boldsymbol{r}) - \theta|^2\}. \tag{3.3}$$

Usually, it is advantageous to have an unbiased estimate with small variance. However a biased estimate with small statistical variations may in some circumstances be more advantageous than an unbiased estimated with large statistical variations. Another convenient performance measure then is the mean square error (MSE) between the estimate and its true value. The lower the MSE, the better the estimate. In the case of unbiased estimates, the MSE becomes the variance of the estimate.

ML Estimator

To introduce the *ML estimator*, the *log likelihood* function (LLF) is first defined as the natural logarithm of the probability density function $p(\boldsymbol{r};\theta)$, taken as a function of θ. Since the logarithm is a monotonically increasing function, the maximum of the LLF will occur at the same location as the maximum of its logarithm. Note that $p(\boldsymbol{r};\theta)$ is not a conditional pdf since the parameter θ is non-random. The log likelihood $\ell(\boldsymbol{r};\theta)$ is thus given by

$$\ell(\boldsymbol{r};\theta) \equiv \ln p(\boldsymbol{r};\theta). \tag{3.4}$$

By definition, the maximum likelihood estimate, denoted by $\hat{\theta}_{\text{ML}}(\boldsymbol{r})$, is the value of θ that maximizes (3.4). In other words, $\hat{\theta}_{\text{ML}}(\boldsymbol{r})$ is chosen such that it maximizes the likelihood of having observed $\boldsymbol{r}$:

$$\hat{\theta}_{\text{ML}}(\boldsymbol{r}) \equiv \arg\max_{\theta} \ell(\boldsymbol{r};\theta). \tag{3.5}$$

A necessary condition for this equation to hold is that the first partial derivative of the log likelihood function with respect to the parameter is null at $\hat{\theta}_{\text{ML}}(\boldsymbol{r})$, i.e.:

$$\left.\frac{\partial \ell(\boldsymbol{r};\theta)}{\partial \theta}\right|_{\theta=\hat{\theta}_{\text{ML}}(\boldsymbol{r})} = 0. \tag{3.6}$$

Unfortunately, local minima may exist in (3.4) such that the above condition is not sufficient. Note that it may be impossible to obtain a closed form expression for $\hat{\theta}_{\text{ML}}(\boldsymbol{r})$ and numerical optimization techniques [20] may be needed to solve (3.5).

ML Multiple Parameter Estimation

The problem of estimating $M > 1$ parameters from the same set of N observations is now addressed. Let $\boldsymbol{\theta} = [\theta^1, \theta^2, \ldots, \theta^M]^T$ be the vector of unknown parameters to be estimated and let the partial derivative vector operator be defined as

$$\boldsymbol{\nabla}_{\boldsymbol{\theta}} = \left[\frac{\partial}{\partial\theta^1}, \frac{\partial}{\partial\theta^2}, \ldots, \frac{\partial}{\partial\theta^M}\right]^T. \tag{3.7}$$

The ML estimate is then the value of $\boldsymbol{\theta}$ that maximizes the LLF, denoted by $\ell(\boldsymbol{r};\boldsymbol{\theta})$. The ML estimate may be obtained by solving the likelihood equation:

$$\boldsymbol{\nabla}_{\boldsymbol{\theta}}\left[\ell(\boldsymbol{r};\boldsymbol{\theta})\right]\big|_{\boldsymbol{\theta}=\hat{\boldsymbol{\theta}}_{\text{ML}}(\boldsymbol{r})} = \mathbf{0}, \tag{3.8}$$

where $\hat{\boldsymbol{\theta}}_{\text{ML}}(\boldsymbol{r})$ is the vector containing the M parameter estimates $\hat{\theta}^m_{\text{ML}}(\boldsymbol{r})$:

$$\hat{\boldsymbol{\theta}}_{\text{ML}}(\boldsymbol{r}) = \left[\hat{\theta}^1_{\text{ML}}(\boldsymbol{r}), \hat{\theta}^2_{\text{ML}}(\boldsymbol{r}), \ldots, \hat{\theta}^M_{\text{ML}}(\boldsymbol{r})\right]^T. \tag{3.9}$$

As it can be seen, the approach is essentially the same for single and multiple parameters estimation.

Cramér-Rao Bound

The Cramér-Rao inequality gives a lower bound on the variance of any unbiased estimate, based on the problem definition. It is a general lower bound that applies to the problem itself and not on a particular estimator function. To verify the performance of an unbiased estimate, its variance is measured or computed and compared to the Cramér-Rao bound (CRB). It is usually desired to have an estimate with a variance as close as possible to the CRB. Any unbiased estimate that achieves the lower bound is called an *efficient* estimate.

First consider the case of a single parameter θ. If $\hat{\theta}(\boldsymbol{r})$ is any unbiased estimate of θ, then if the first and second partial derivatives of the pdf $p(\boldsymbol{r};\theta)$ with respect to θ exist and are absolutely

integrable [9], the variance of the estimate is limited by the Cramér-Rao lower bound:

$$Var[\hat{\theta}(\boldsymbol{r})] \geq -E\left\{\left[\frac{\partial^2 \ell(\boldsymbol{r};\theta)}{\partial^2 \theta}\right]\right\}^{-1}. \tag{3.10}$$

According to this equation, any (unbiased) estimate *must* have a variance greater than the Cramér-Rao lower limit as given by the right hand side of (3.10).

It can be shown that if an efficient estimate exists, it is given by the maximum likelihood estimate $\hat{\theta}_{\text{ML}}(\boldsymbol{r})$. Furthermore, it can be proven that the ML estimate is asymptotically efficient [9], that is: as the number N of observation samples increases, the variance of the ML estimate approaches the Cramér-Rao bound. This property provides a strong justification for using the ML estimator in practice.

For multiple parameters estimation, i.e. $\boldsymbol{\theta} = [\theta^1, \theta^2, \ldots, \theta^M]^T$, the Cramér-Rao bound is obtained through the inversion of the so-called Fisher information matrix $\boldsymbol{J}$, which is defined as the $M \times M$ matrix with element (i, j) such that

$$J_{i,j} = E\left[\frac{\partial \ell(\boldsymbol{r};\boldsymbol{\theta})}{\partial \theta^i} \cdot \frac{\partial \ell(\boldsymbol{r};\boldsymbol{\theta})}{\partial \theta^j}\right] \tag{3.11a}$$

$$= -E\left[\frac{\partial^2 \ell(\boldsymbol{r};\boldsymbol{\theta})}{\partial \theta^i \partial \theta^j}\right], \tag{3.11b}$$

where the second equality, follows from the properties of the integral of the pdf $p(\boldsymbol{r};\theta)$ [9]. The lower bound on the variance of individual estimates is then given by

$$Var[\hat{\theta}^m_{\text{ML}}(\boldsymbol{r})] \geq [\boldsymbol{J}^{-1}]_{m,m} \tag{3.12}$$

where $[\boldsymbol{J}^{-1}]_{i,j}$ denotes the element (i, j) of the inverse of $\boldsymbol{J}$ and m denotes the parameter index.

3.2 Joint Parameters Estimator

The joint ML estimator for the channel parameters introduced in Chapter 2 is now derived. In particular, it is required to estimate $|\psi|$, $\measuredangle\psi$, τ and ϵ, as defined in sections 2.2 and 2.3, given the observation of N received samples. Recall that ψ represents the complex reflection coefficient, $|\psi|$ and $\measuredangle\psi$ are its magnitude and angle respectively, τ represents a time delay and ϵ the synchronization offset.

First, the probability model for the system needs to be derived. Once the probability density function is known, the log likelihood function can be directly obtained and it becomes possible to derive the joint ML estimator. Then, having the joint ML estimator, its performance can be investigated. The mean and variance of the ML estimate are discussed in this section, while the study of the CRB is postponed until section 3.4.

3.2.1 Probability Model

In this section, the probability model of the communication system under study is derived. More specifically, the joint probability density function $p(\boldsymbol{x};\boldsymbol{\theta})$ is derived, where

$$\boldsymbol{\theta} = [|\psi|, \measuredangle\psi, \tau, \epsilon]^T \tag{3.13}$$

is the vector of unknown parameters to be estimated and $\boldsymbol{x}$ is the vector of data observations, defined later. The information available at the receiver for the estimation is the received signal in (2.33), with the tilde " ˜ " removed for clarity, over an observation period of duration T_o that may span several symbol durations (i.e. $T_\text{o} \gg T$):

$$r(t) = u(t) + v(t), \quad 0 \leq t \leq T_\text{o}, \tag{3.14}$$

where $v(t)$ is defined in (2.34) with power spectral density (2.42) and $u(t)$ is the mean of $r(t)$, given by

$$u(t) = \sum_{k=-\infty}^{\infty} \sum_{l=0}^{\infty} \psi^l A_k g(t - kT - 2l\tau - \epsilon). \tag{3.15}$$

Notice that the synchronization offset ϵ is now integrated in $u(t)$, even if the offset does not occur until sampling. This is a modelling convenience which allows the parameter to be estimated using the continuous-time signal. This has no effects on the implementation since it is performed in discrete-time, where the synchronization offset is necessarily present.

To simplify the development of the ML estimates, $r(t)$ is represented using a discrete set (and ideally finite) of related observations. A common approach in the literature is to use the Fourier series coefficients [13, 12]. As such, the Fourier series representation of $r(t)$ in (3.14) is given by:

$$R(\omega_q) \triangleq \frac{1}{T_\text{o}} \int_0^{T_\text{o}} r(t) e^{-j\omega_q t} dt, \qquad \omega_q = \frac{2\pi q}{T_\text{o}}, \quad q \in \mathbb{Z}. \tag{3.16}$$

The Fourier series representation is a one-to-one transformation; it is possible to recover the original observation signal $r(t)$ from the set of $R(\omega_q)$. Thus, $R(\omega_q)$ contains all the information contained in $r(t)$. In this application, the signal $r(t)$ is bandlimited to $W = \pm\frac{(1+\beta)\pi}{T}$ so that

$$R(\omega_q) \simeq 0 \qquad \text{for } |q| > Q, \quad Q = \left\lceil \frac{WT_{\text{o}}}{2\pi} \right\rceil, \tag{3.17}$$

where $\lceil t_0 \rceil$ is the largest integer less than or equal to t_0.

Recall from Chapter 2 that $r(t)$ is Gaussian. Accordingly, $R(\omega_q)$ are complex Gaussian random variables. Let the mean of the Fourier series coefficients be

$$U(\omega_q) \triangleq E[R(\omega_q)], \tag{3.18}$$

then if the observation time bandwidth product is large, i.e. the observation time is much longer than the symbol period or equivalently $WT_{\text{o}} \gg 2\pi$, it can be shown (e.g. [13,21]) that the Fourier coefficients corresponding to different frequencies are uncorrelated, specifically

$$E[(R(\omega_q) - U(\omega_q))(R(\omega_p) - U(\omega_p))^*] \simeq P_q \delta[q-p] \tag{3.19}$$

$$E[(R(\omega_q) - U(\omega_q))(R(\omega_p) - U(\omega_p))] = 0, \tag{3.20}$$

where $P_q = S_v(\omega_q)/T_{\text{o}}$ and $S_v(\omega)$ is the noise power spectral density defined in (2.42). Therefore, the coefficients in $R(\omega_q)$ in (3.16) are complex circular Gaussian [19] and the probability density function of the data can be obtained by first defining the data and mean vectors, respectively:

$$\boldsymbol{x} = [R(\omega_{-Q}), \ldots, R(\omega_Q)]^T \tag{3.21}$$

$$\boldsymbol{y} = [U(\omega_{-Q}), \ldots, U(\omega_Q)]^T. \tag{3.22}$$

The probability density function $p(\boldsymbol{x}; \boldsymbol{\theta})$ is finally expressed as

$$p(\boldsymbol{x}; \boldsymbol{\theta}) = \frac{1}{\pi^Q |\boldsymbol{K}|} \exp\left\{ -(\boldsymbol{x} - \boldsymbol{y})^H \boldsymbol{K}^{-1} (\boldsymbol{x} - \boldsymbol{y}) \right\}, \tag{3.23}$$

where $\boldsymbol{K}$ is defined as the diagonal matrix with elements P_q, i.e.:

$$\boldsymbol{K} = \mathrm{diag}[P_{-Q}, \ldots, P_Q] = \begin{bmatrix} P_{-Q} & \cdots & 0 \\ \vdots & \ddots & \vdots \\ 0 & \cdots & P_Q \end{bmatrix} \tag{3.24}$$

and $|\boldsymbol{K}|$ is its determinant.

3.2.2 ML Estimator

To get the ML estimator, the logarithm of (3.23) is taken to obtain the log likelihood function $\ell(\boldsymbol{x};\boldsymbol{\theta})$:

$$\ell(\boldsymbol{x};\boldsymbol{\theta}) \triangleq -\log(\pi^Q|\boldsymbol{K}|) - (\boldsymbol{x}-\boldsymbol{y})^H\boldsymbol{K}^{-1}(\boldsymbol{x}-\boldsymbol{y}). \tag{3.25}$$

Notice that $\boldsymbol{K}$ is independent of the parameters so that the term containing its determinant in (3.25) may be ignored since it will be nulled later by the maximization procedure. Therefore, the log likelihood equation becomes:

$$\begin{aligned} \ell(\boldsymbol{x};\boldsymbol{\theta}) &= -\sum_{m=-Q}^{Q} (R(\omega_q) - U(\omega_q))^* \frac{1}{P_q} (R(\omega_q) - U(\omega_q)) \\ &= -T_{\mathrm{o}} \sum_{m=-Q}^{Q} \frac{|R(\omega_q) - U(\omega_q)|^2}{S_v(\omega_q)} \end{aligned} \tag{3.26}$$

To obtain the ML estimator, (3.26) must be maximized with respect to the parameter $\boldsymbol{\theta}$, or equivalently $\tilde{\ell}(\boldsymbol{x};\boldsymbol{\theta}) = -\ell(\boldsymbol{x};\boldsymbol{\theta})$ must be minimized. Note that here, the dependence on the parameter vector is through the frequency coefficients $U(\omega_q)$, that is

$$U(\omega_q) \equiv U(\omega_q;\boldsymbol{\theta}). \tag{3.27}$$

Two interpretations of (3.26), which lead to different ML estimator structures, are now proposed followed by an approximate solution, based on the discrete-time domain received signal in (2.35).

First Interpretation

Recall from Chapter 2 that the raised cosine spectrum $G(\omega)$ in (2.19) is real and symmetric and that $G(\omega) = P(\omega)P^*(\omega)$, where $P(\omega)$, the square root of the raised cosine spectrum, is also real and symmetric. Then, the noise power spectral density in (2.42) may be expressed as

$$S_v(\omega_q) = N_o P(\omega_q) P^*(\omega_q). \tag{3.28}$$

Then, the negative of the log likelihood function can be expressed as follows

$$\tilde{\ell}(\boldsymbol{x};\boldsymbol{\theta}) = \frac{T_o}{N_o} \sum_{q=-Q}^{Q} |V(\omega_q)|^2, \tag{3.29}$$

where $V(\omega_q)$ is given by

$$V(\omega_q) = \frac{1}{P(\omega_q)} \left[R(\omega_q) - U(\omega_q;\boldsymbol{\theta}) \right]. \tag{3.30}$$

The ML estimate is then the parameter $\boldsymbol{\theta}$ that minimizes the power of the signal $V(\omega_q)$. Figure 3.1 illustrates the ML processor in the time domain. The filter with frequency response $\frac{1}{P(\omega)}$ corresponds to a pre-whitening filter. The parameters ψ, τ and ϵ are selected to minimize the output of the illustrated system, by making the weighted difference between $u(t)$ and $r(t)$ small. Notice that the constant multiplicative factor T_o/N_o is independent of the parameter and does not require to be considered in the minimization.

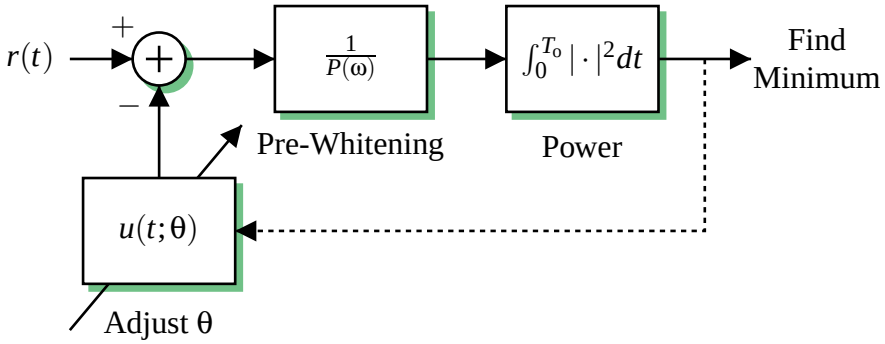

Fig. 3.1 ML Estimator Structure I (Power minimization)

Second Interpretation

The second interpretation of (3.26) is obtained by expanding its magnitude squared term. Equivalently, the magnitude squared term of $\tilde{\ell}(\boldsymbol{x};\boldsymbol{\theta})$ can be expanded resulting in four terms:

$$\tilde{\ell}(\boldsymbol{x};\boldsymbol{\theta}) = \ell_{11} + \ell_{12} + \ell_{21} + \ell_{22}. \tag{3.31}$$

The first term, ℓ_{11}, corresponds to the weighted sum of the data magnitude squared, i.e.:

$$\ell_{11} = T_{\text{o}} \sum_{q=-Q}^{Q} \frac{|R(\omega_q)|^2}{S_v(\omega_q)}. \tag{3.32}$$

This term is independent of the parameter $\boldsymbol{\theta}$. Consequently, it has no effects in the minimization of $\tilde{\ell}(\boldsymbol{r};\boldsymbol{\theta})$ and can be ignored.

The two middle terms in (3.31) are complex conjugates of each other. Their sum corresponds exactly to twice the real part of ℓ_{12}. The term ℓ_{12} is given by

$$\begin{aligned} \ell_{12} &= -\frac{T_{\text{o}}}{N_o} \sum_{q=-Q}^{Q} \frac{R(\omega_q)}{P(\omega_q)} \frac{U^*(\omega_q)}{P^*(\omega_q)} \\ &= -\frac{1}{N_o} \int_0^{T_{\text{o}}} r_w(t) u_w^*(t) dt, \end{aligned} \tag{3.33}$$

where $r_w(t)$ and $u_w(t)$ are the "whitened" version of the received and the mean signal, respectively. The received whitened signal $r_w(t)$ is obtained through convolution of $r(t)$ with a whitening filter that has frequency response $1/P(\omega)$. To get $u_w(t)$, filtering is not necessary; the same result may be obtained by using $p(t)$ instead of $g(t)$ when reconstructing the mean in (3.15), i.e.:

$$u_w(t) \equiv u_w(t;\boldsymbol{\theta}) = \sum_{k=-\infty}^{\infty} \sum_{l=0}^{\infty} \psi^l A_k p(t - kT - 2l\tau - \epsilon), \tag{3.34}$$

where once again the dependence on the parameter $\boldsymbol{\theta}$ is clearly indicated.

The last term in (3.31), ℓ_{22}, corresponds to the energy of the mean signal $u(t)$ scaled by the

inverse noise power spectral density, and it is given by

$$\begin{aligned}\ell_{22} &= T_o \sum_{q=-Q}^{Q} \frac{|U(\omega_q)|^2}{S_v(\omega_q)} \\ &= \ell_{22}(\boldsymbol{\theta}).\end{aligned} \tag{3.35}$$

This term is independent of the data but depends on the parameters and will affect the minimization.

Figure 3.2 shows the implementation of this interpretation of the ML estimator. The objective of the ML estimator is then to find the value of $\boldsymbol{\theta}$ that minimizes the output of the system illustrated. This structure can be interpreted as a generalized correlator where the parameter $\boldsymbol{\theta}$ that gives the highest correlation between $u_w(t;\boldsymbol{\theta})$ and $r(t)$ corresponds to the maximum likelihood estimate.

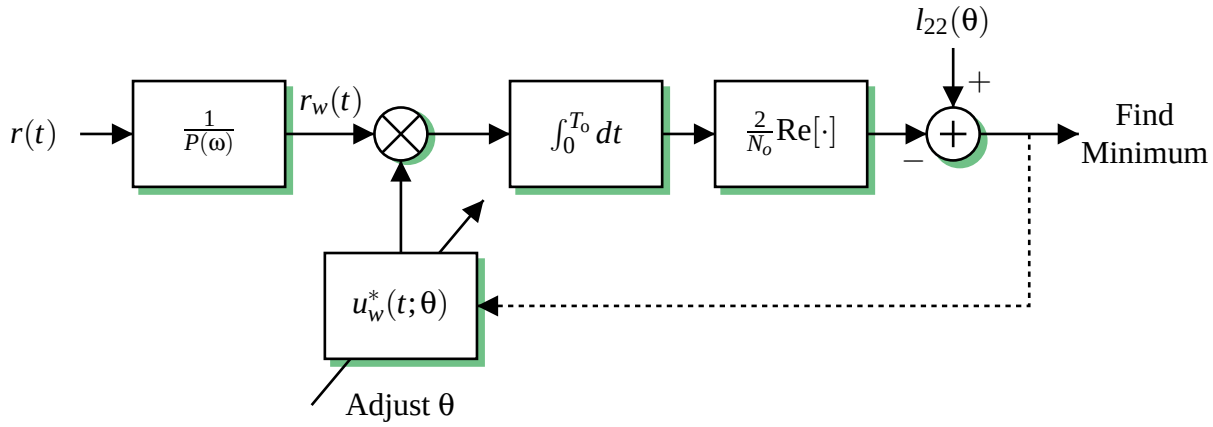

Fig. 3.2 ML Estimator Structure II (Generalized correlator)

Approximate ML

The previous interpretations of the ML estimator are based on a continuous-time domain model. In practice, the estimation would be performed numerically, using a set of discrete-time observations. Some approximations are therefore necessary to develop a practical discrete-time ML estimator.

It is first noted from the structure of the radio unit in Fig. 2.4 that no pre-whitening filter is

available at the receiver. Consequently, the higher frequencies, attenuated by the spectral shape of the raised cosine, will not be enhanced. Therefore, it is assumed here that the portion of the signal energy located in the excess bandwidth, i.e. $\pi/T < |\omega| < W$, is negligible.

This assumption allows to use the symbol-spaced samples, available at the receiver, to completely represent the continuous-time signal, $r(t)$. Let $r[n]$ represent the set of symbol-spaced samples such that (2.35) becomes

$$r[n] = u[n] + v[n], \tag{3.36}$$

where $u[n]$ is given by

$$u[n] \equiv u[n;\boldsymbol{\theta}] = \sum_{k=-\infty}^{\infty} \sum_{l=0}^{\infty} \psi^l A_k g((n-k)T - 2l\tau - \epsilon) \tag{3.37}$$

and the change of index (from m to n) indicates the change of sampling rate. The noise term $v[n] = v(nT)$ is zero-mean circular Gaussian and has autocorrelation function $R_v[n]$ defined as

$$R_v[n] = N_o g(n) = N_o \delta[n]. \tag{3.38}$$

Since it is assumed that the set of $r[n]$, $n = \{0, 1, \ldots, N-1\}$, forms a complete representation for $r(t)$, $0 \leq t \leq T_o = NT$, the integral in Fig. 3.1 and Fig. 3.2 for the computation of power may be replaced by a sum over the discrete-time samples. The attention will be focused on the equivalent of Structure I for the approximate ML estimator. The consequences for Structure II are similar and will not be considered here.

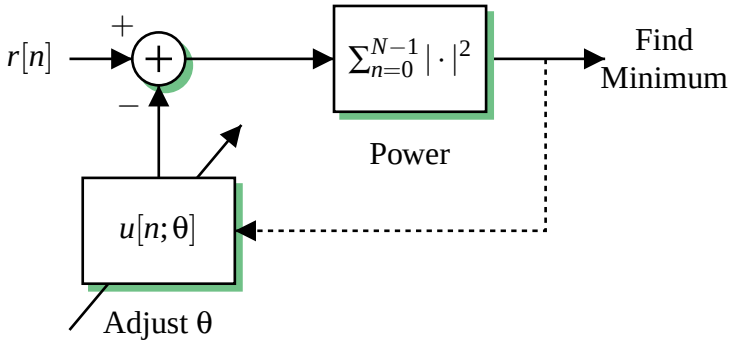

Fig. 3.3 Approximate ML Estimator

Figure 3.3 illustrates the proposed approximate ML estimator. The estimation is performed in the time-domain, using the symbol-spaced samples. Notice that the radio unit under consideration uses half-spaced samples. So half the samples are not considered in this approximation for the reasons mentioned above. The approximate ML estimator minimizes the power of the difference between the re-created signal $u[n]$ based on the parameters $\boldsymbol{\theta}$ and the received samples $r[n]$. The maximization algorithm must find the value of $\boldsymbol{\theta}$ that maximizes the following log likelihood function, obtained in the same way as (3.26):

$$\ell(\boldsymbol{r};\boldsymbol{\theta}) = -\frac{1}{N_o}(\boldsymbol{r}-\boldsymbol{u})^H(\boldsymbol{r}-\boldsymbol{u}), \tag{3.39}$$

where $\boldsymbol{r}$ and $\boldsymbol{u}$ are the data and mean vectors defined respectively as

$$\boldsymbol{r} = [r[0], r[1], \ldots, r[N-1]]^T \tag{3.40}$$

$$\boldsymbol{u} = [u[0], u[1], \ldots, u[N-1]]^T. \tag{3.41}$$

The ML estimate $\boldsymbol{\theta}_{\text{ML}}(\boldsymbol{r})$ is therefore given by the following expression,

$$\hat{\boldsymbol{\theta}}_{\text{ML}}(\boldsymbol{r}) = \arg\min_{\boldsymbol{\theta}} |\boldsymbol{r}-\boldsymbol{u}|^2, \tag{3.42}$$

which may be solved by using a multi-dimensional search for the parameter $\boldsymbol{\theta}$. Practical solution of this equation is treated later in section 3.3.

Estimator Performance

Comments will now be given on the performance of the ML estimator. In particular, the mean and variance of the estimate obtained through the use of the estimator function are discussed.

There is no explicit expression for $\hat{\boldsymbol{\theta}}_{\text{ML}}(\boldsymbol{r})$ so the mean cannot be computed in closed form. However, from (3.42) it can be seen that the closer the vector $\boldsymbol{u}$ is from the actual received vector $\boldsymbol{r}$, the better the estimation is. In fact, the estimation procedure tries to "recreate" the signal that would have been received given a certain set of parameters $\boldsymbol{\theta}$. Therefore, if the model for $\boldsymbol{u}$ is accurate enough and if the noise is zero-mean, the estimates will be unbiased.

Unfortunately, the vector $\boldsymbol{u}$ is obtained through a double summation over an infinite number of terms, impossible to perform in practice. Consequently, the model for the received signal can only be approximated by limiting those sums in (3.37). If the limits for the indices k and l in

(3.37) are chosen judiciously, it can be assumed that the effects of the finite sums are negligible and that the model accurately represents the system. Under this condition, the argument in (3.42) on average would go to zero, leading to the conclusion the estimates obtained are unbiased. The results on the iterative estimator in Chapter 5 clearly confirm the validity of these assumptions.

Again, there is no explicit expression for $\hat{\boldsymbol{\theta}}_{\mathrm{ML}}(\boldsymbol{r})$ so the variance cannot be computed in closed form. The estimates' variance are therefore obtained through simulations. A theoretical lower bound on the variances is available through the Cramér-Rao bound, which is developed in section 3.4.

3.3 Practical Considerations

The core of the parameter estimation approach resides in the solution of (3.42). Practical ways of solving the joint parameter ML estimator are therefore presented in this section. Since the joint ML estimator involves finding the minimum of a non-linear function, it cannot be solved directly through simple substitution. Consequently, optimization theory is used to find the ML estimates. First, a block optimization procedure will be considered, where N samples are used to compute the ML estimates. Then, an iterative approach will be introduced, where an estimate of the parameters is available after every sample.

3.3.1 Block Estimator

The routine for block estimation consists of gathering N samples in an observation vector $\boldsymbol{r}$, and use it in the optimization procedure, as illustrated in Fig 3.4. Since the optimization requires

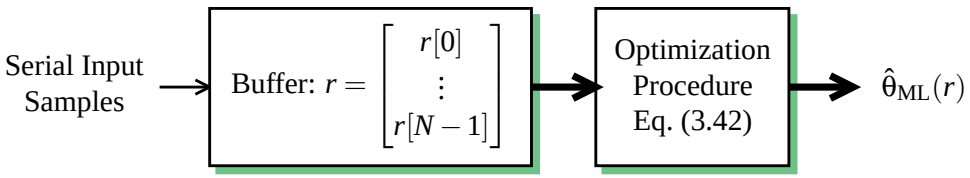

Fig. 3.4 Block Estimation

N samples at a time, there is a delay of at least N samples before the first set of estimates is made available. In practice, the delay is even longer since the procedure itself takes some time to produce the estimates.

It is possible to obtained a numerical solution of (3.42) by using a multi-dimensional optimization algorithm [20]. In this respect, the parameter space for the search may be bounded, according to the parameters' physical meaning, i.e.:

- $|\psi|$ represents the magnitude of the reflection coefficient. Since a negative value of the magnitude does not have a physical meaning and a value larger than 1 would mean that there is amplification on the transmission line, necessarily $0 \leq |\psi| < 1$.

- $\measuredangle\psi$ is the phase of the reflection coefficient. By definition $-\pi < \measuredangle\psi \leq \pi$.

- τ represents the time delay required for the wave to travel to the end of the transmission line. Physically, this must be a positive value. It is further assumed that $\tau_{min} \leq \tau \leq \tau_{max}$ where τ_{min} represents the minimum time delay and τ_{max} represents the maximum time delay. The minimum time delay is related to the minimum cable length possible for proper operation. The cable must connect the receiver to the antenna and since the latter is usually located at some height above the ground on top of a tower structure, knowing the minimum height of the tower, the minimum cable length can be found. The maximum time delay τ_{max} is related to the length of the transmission line; for very long cable, the attenuation would make the reflection magnitude negligible compared to that of the noise level and it would not distort the received signal significantly.

- ϵ represents the synchronization offset and may also be bounded; its value must be such that $-T/4 < \epsilon \leq T/4$ for half-spaced sampling since otherwise the synchronizer would lock on the adjacent half-symbol.

  Closer bounds for ϵ can be found by using the fact that it is a semi-predictable synchronization offset dependent on ψ and τ. For instance, using the limiting cases for $|\psi|$, $\measuredangle\psi$ and τ, i.e. $0 \leq |\psi| < 1$, $-\pi < \measuredangle\psi \leq \pi$ and $\tau_{\text{min}} \leq \tau \leq \tau_{\text{max}}$, in a synchronization algorithm (e.g. correlation), the range of ϵ could be found more precisely.

In general, a finite search space for $\boldsymbol{\theta}$ can be determined. Since (3.42) is non-linear in $\boldsymbol{\theta}$, the optimization algorithm to use in this case must be a non-linear constrained algorithm. The constraint consists of the parameters' bounds. Straightforward procedures exists for solving these types of problems, including the *downhill simplex method* and *Powell's method* [22]. More complex optimization software use a set of different steps to solve an optimization problem and are general enough to be applicable to a number of different problems. The block optimization procedure

used in this work is presented in the documentation of the numerical computation software used in [23]. No more details will be given on optimization methods as they are beyond the scope of this work. Nevertheless, a detailed discussion on the subject can be found in [20]. Note that non-linear optimization procedures can be very computationally demanding.

3.3.2 Iterative Estimator

The previous section discussed a method that solves (3.42) using a block approach, which involves a long delay and a computationally intensive optimization procedure. Alternatively, an iterative approach based on the steepest descent algorithm can be used. This approach produces a new estimate every sample and does not require a complex optimization procedure. It is also advantageous for use in non-stationary environment. This joint iterative estimator is derived next, starting from the steepest descent algorithm.

Steepest Descent Algorithm

The steepest descent algorithm is a general non-linear optimization technique [20] that originates from the optimization of quadratic problems. It can be applied to general non-linear problems as well, often with good results. Although it has a relatively slow convergence rate, it is guaranteed to converge to at least a local minimum. The standard steepest descent algorithm for a vector of parameter $\boldsymbol{\theta}$ is defined as [20]:

$$\boldsymbol{\theta}_{n+1} = \boldsymbol{\theta}_n + \mu_n \boldsymbol{\nabla}_{\boldsymbol{\theta}} \ell(\boldsymbol{r}; \boldsymbol{\theta}_n), \tag{3.43}$$

where $\boldsymbol{\theta}_n$ represents the vector of parameters at time index n and μ_n is a time-dependent step-size chosen so that

$$\mu_n = \arg\max_{\mu} \ell\left(\boldsymbol{r}; \boldsymbol{\theta}_n + \mu \boldsymbol{\nabla}_{\boldsymbol{\theta}} \ell(\boldsymbol{r}; \boldsymbol{\theta}_n)\right). \tag{3.44}$$

The estimate $\hat{\boldsymbol{\theta}}$ is obtained through iteration of (3.43) until convergence.

Joint Iterative Estimator

The steepest descent algorithm described above is a "block" technique in the sense that it operates on a vector of observations $\boldsymbol{r}$ and iterates until it converges for that block of observations. Here, a different approach is proposed, where the iterative algorithm only uses one sample at a time.

Specifically, the gradient of the log likelihood function in (3.43) is first applied to (3.39), which leads to the following equation:

$$\boldsymbol{\nabla}_{\boldsymbol{\theta}}\ell(\boldsymbol{r};\boldsymbol{\theta}) = \boldsymbol{\nabla}_{\boldsymbol{\theta}}\left(-\frac{1}{N_o}(\boldsymbol{r}-\boldsymbol{u})^H(\boldsymbol{r}-\boldsymbol{u})\right). \tag{3.45}$$

Recall that $\boldsymbol{r}$ is independent of $\boldsymbol{\theta}$ thus the gradient with respect to parameter m of the log likelihood at iteration n becomes:

$$\frac{\partial}{\partial\theta^m}\ell(\boldsymbol{r};\boldsymbol{\theta}_n) = \frac{2}{N_o}\text{Re}\left[\frac{\partial\boldsymbol{u}^H}{\partial\theta^m}(\boldsymbol{r}-\boldsymbol{u})\right]\Bigg|_{\boldsymbol{\theta}=\boldsymbol{\theta}_n}. \tag{3.46}$$

Since it would be difficult to solve (3.44) for the step size μ, we propose to use a fixed step size μ^m, different for each parameter. The algorithm then becomes for each parameter m:

$$\theta^m_{n+1} = \theta^m_n + \mu^m\frac{\partial}{\partial\theta^m}\ell(\boldsymbol{r};\boldsymbol{\theta}_n). \tag{3.47}$$

For each iteration of the search algorithm, the entire vector $\boldsymbol{r}$ of N observations is required. Consequently, (3.47) is further modified so that only one observation sample is used and one iteration is performed at every time instant. The joint iterative parameter estimator is then expressed as

$$\theta^m_{n+1} = \theta^m_n + \mu^m\frac{\partial}{\partial\theta^m}\ell(r[n];\boldsymbol{\theta}_n), \tag{3.48}$$

where the gradient of the log likelihood now acts on a single received sample and is now defined as

$$\frac{\partial}{\partial\theta^m}\ell(r[n];\boldsymbol{\theta}_n) = 2\text{Re}\left[\frac{\partial}{\partial\theta^m}(u^*[n])(r[n]-u[n])\right]\Bigg|_{\boldsymbol{\theta}=\boldsymbol{\theta}_n}, \tag{3.49}$$

where the factor T/N_o is absorbed by the corresponding step-size in (3.48). The procedure is illustrated in Fig 3.5, where the vector $\boldsymbol{\mu}$ is the step-size vector, i.e.:

$$\boldsymbol{\mu} = [\mu^1\mu^2\mu^3\mu^4]^T, \tag{3.50}$$

and the vector multiplication is performed element by element.

It has been observed through experimentation that some parameters have a better convergence than others. In particular, $|\psi|$ and $\measuredangle\psi$ showed good convergence properties even in the absence of good estimates for τ and ϵ. This can be exploited by updating the estimates of $|\psi|$ and $\measuredangle\psi$ first

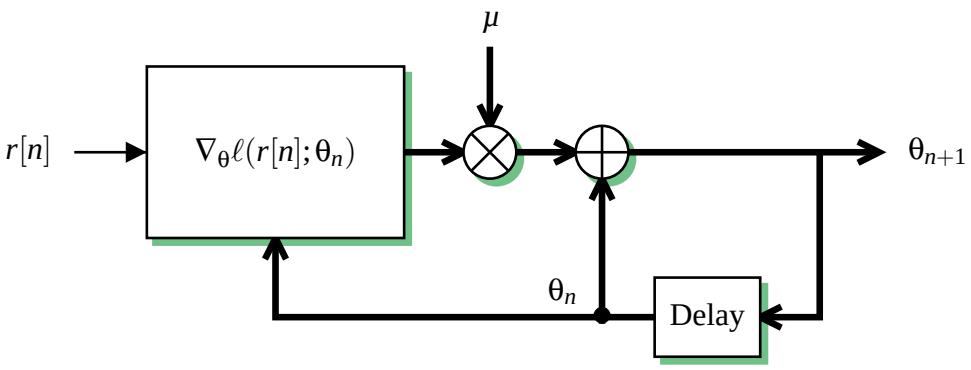

Fig. 3.5 Iterative Estimation Procedure

and then use those new estimates to update the other two parameters estimates. It is possible to do so by making use of the structure of (3.48). First, new notation is introduced for $u[n]$; it may be separated in the following way:

$$u[n] = \sum_{l=0}^{\infty} \psi^l \upsilon[n;l] \tag{3.51}$$

where $\upsilon[n;l]$ is given by

$$\upsilon[n;l] = \sum_{k=-\infty}^{\infty} A_k g((n-k)T - 2l\tau - \epsilon). \tag{3.52}$$

Note that the sums in (3.51) and (3.52) would have to be truncated so that numerical computation may be possible. The computation of the gradient of the log likelihood in (3.49) also requires the

first derivative of $u[n]$ with respect to each parameter, which are given below:

$$u_1[n] = \sum_{l=0}^{\infty} l\frac{\psi^l}{|\psi|}\upsilon[n;l] \tag{3.53a}$$

$$u_2[n] = \sum_{l=0}^{\infty} jl\psi^l\upsilon[n;l] \tag{3.53b}$$

$$u_3[n] = -\sum_{l=0}^{\infty} 2l\psi^l\upsilon'[n;l] \tag{3.53c}$$

$$u_4[n] = -\sum_{l=0}^{\infty} \psi^l\upsilon'[n;l], \tag{3.53d}$$

where $u_i[n]$ represents the first derivative of $u[n]$ with respect to parameter at index i in (3.13) and $\upsilon'[n;l]$ is the first derivative of $\upsilon[n;l]$ and is given by

$$\upsilon'[n;l] = \sum_{k=-\infty}^{\infty} A_k g'(nT - kT - 2l\tau - \epsilon). \tag{3.54}$$

By definition, $\upsilon[n;l]$ and $\upsilon'[n;l]$ depend on both τ and ϵ but are independent of $|\psi|$ and $\measuredangle\psi$. As a result, $\upsilon[n;l]$ and $\upsilon'[n;l]$ can be computed first, for $l = \{0, 1, \ldots, L\}$ at each instant n. The choice of L depends on the expected $|\psi|$, the noise power and the desired precision of the estimates. For example, it was found by experimentation that $L = 3$ gives satisfactory estimates, for a SNR of 20dB and $|\psi| = 0.1$.

Once $\upsilon[n;l]$ and $\upsilon'[n;l]$ are available, the estimates for $|\psi|$ and $\measuredangle\psi$ can then be updated using (3.48). Using those new values, the estimates for τ and ϵ are then computed. The procedure is repeated for every new sample. Algorithm 3.1 exposes the full process.

The iterative algorithm presented here is an approximation to the joint ML parameter estimator in (3.42). Nevertheless, this scheme is attractive for high speed modems where the computational capacity is limited. For this type of application, the extra convergence time may not be a problem and this algorithm may be adequate. Note also that the algorithm can be directly extended to make use of the half samples as well in fractionally spaced digital modems.

Algorithm 3.1 Iterative Parameter Estimation

Let $\boldsymbol{\theta}_n \equiv [\theta_n^{|\psi|}, \theta_n^{\measuredangle\psi}, \theta_n^{\tau}, \theta_n^{\epsilon}]^T = [\theta_n^1, \theta_n^2, \theta_n^3, \theta_n^4]^T$.

$n \leftarrow 0$
$\boldsymbol{\theta}_0 \leftarrow \mathbf{0}$
Assign to μ^m a small positive constant for $m \in \{1, 2, 3, 4\}$
loop
  Compute $u[n; l]$ using $\boldsymbol{\theta}_n$ and (3.52) for $l \in \{0, 1, \ldots, L\}$
  Compute $u'[n; l]$ using $\boldsymbol{\theta}_n$ and (3.54) for $l \in \{0, 1, \ldots, L\}$

  Update $\theta_{n+1}^{|\psi|}$ using $\theta_n^{|\psi|}$, $\theta_n^{\measuredangle\psi}$, (3.48) and (3.53a)
  Update $\theta_{n+1}^{\measuredangle\psi}$ using $\theta_{n+1}^{|\psi|}$, $\theta_n^{\measuredangle\psi}$, (3.48) and (3.53b)
  Update θ_{n+1}^{τ} using $\theta_{n+1}^{|\psi|}$, $\theta_{n+1}^{\measuredangle\psi}$, (3.48) and (3.53c)
  Update θ_{n+1}^{ϵ} using $\theta_{n+1}^{|\psi|}$, $\theta_{n+1}^{\measuredangle\psi}$, (3.48) and (3.53d)

  $\boldsymbol{\theta}_{n+1} \Leftarrow [\theta_{n+1}^{|\psi|}, \theta_{n+1}^{\measuredangle\psi}, \theta_{n+1}^{\tau}, \theta_{n+1}^{\epsilon}]^T$
  $n \Leftarrow n + 1$
end loop

3.4 Cramér-Rao Bound

Since the variance of the estimate cannot be computed explicitly, other ways of evaluating it must be used. Using computer simulations, the estimate variances are determined and then compared to the Cramér-Rao lower bound.

The CRB is obtained by inverting the Fisher information matrix with entries (i, j) as defined in (3.11b). The first partial derivative of the log likelihood function in (3.26) with respect to parameter i is given by

$$\frac{\partial \ell(\boldsymbol{x}; \boldsymbol{\theta})}{\partial \theta^i} = \frac{2T_{\mathrm{o}}}{N_o} \sum_{q=-Q}^{Q} \frac{1}{G(\omega_q)} \mathrm{Re}\left[\frac{\partial U(\omega_q)}{\partial \theta^i}(R(\omega_q) - U(\omega_q))^*\right], \tag{3.55}$$

where the noise power spectral density has been replaced by its equivalent, i.e.: $S_v(\omega) = N_o G(\omega)$,and the raised cosine spectrum $G(\omega)$ is defined in (2.19). The second partial derivative of the log like-

lihood function with respect first to parameter θ_i and then to parameter θ_j is given by

$$\frac{\partial^2 \ell(\boldsymbol{r};\boldsymbol{\theta})}{\partial\theta^j\partial\theta^i} = \frac{2T_\mathrm{o}}{N_o}\sum_{q=-Q}^{Q}\frac{1}{G(\omega_q)}\mathrm{Re}\left[\frac{\partial^2 U(\omega_q)}{\partial\theta^j\partial\theta^i}(R(\omega_q)-U(\omega_q))^* - \left(\frac{\partial U(\omega)}{\partial\theta^i}\right)^*\left(\frac{\partial U(\omega)}{\partial\theta^j}\right)\right]. \tag{3.56}$$

Substituting (3.56) in (3.11) and using the fact that $E[R(\omega)] = U(\omega)$ by definition, the element (i,j) of Fisher information matrix becomes:

$$J_{i,j} = \frac{2T_\mathrm{o}}{N_o}\sum_{q=-Q}^{Q}\frac{1}{G(\omega_q)}\mathrm{Re}\left[\left(\frac{\partial U(\omega_q)}{\partial\theta^i}\right)^*\left(\frac{\partial U(\omega_q)}{\partial\theta^j}\right)\right]. \tag{3.57}$$

In Appendix B, it is shown that the Fourier series coefficients of $u(t)$, $0 \le t \le T_\mathrm{o}$ are approximately given by

$$U(\omega_q) \simeq \frac{1}{T_\mathrm{o}}F(\omega_q;\boldsymbol{\theta})G(\omega_q)D(\omega_q), \tag{3.58}$$

where $F(\omega_q;\boldsymbol{\theta}) \equiv F(\omega)$ is the composite channel response, which includes the effects of the channel in (A.7) and the synchronization offset, so that

$$F(\omega) = \frac{1}{2}\tilde{H}(\omega)e^{-j\omega\epsilon} = \frac{e^{-j\omega\epsilon}}{1-\psi^{-j\omega 2\tau}}, \tag{3.59}$$

and $D(\omega_q)$ represents the contribution of the data and is given by

$$D(\omega_q) = \sum_{k=0}^{N-1} A_k e^{-j\omega_q kT}. \tag{3.60}$$

Notice that $D(\omega_q)$ is the discrete Fourier transform (DFT) [25] of A_k, $0 \le k < N$. Substituting (3.58) in (3.57), using the fact that $G(\omega)$ is real and observing that only $F(\omega_q)$ is function of the parameters, $J_{i,j}$ may be expressed as

$$J_{i,j} = \frac{2}{T_\mathrm{o}N_o}\sum_{q=-Q}^{Q} G(\omega_q)|D(\omega_q)|^2\mathrm{Re}\left[F_i^*(\omega_q)F_j(\omega_q)\right], \tag{3.61}$$

where $F_i(\omega_q)$ represents the partial derivative of $F(\omega_q)$ with respect to parameter θ^i, i.e.:

$$F_i(\omega_q) \equiv \frac{\partial F(\omega_q)}{\partial \theta^i}. \tag{3.62}$$

It can be easily shown using the definition of $F(\omega)$ in (3.59) that the partial derivatives in (3.62) are given by

$$F_1(\omega_q) = e^{j\omega_q \epsilon} e^{j\measuredangle\psi} e^{-j\omega_q 2\tau} F^2(\omega_q) \tag{3.63a}$$
$$F_2(\omega_q) = j\psi e^{j\omega_q \epsilon} e^{-j\omega_q 2\tau} F^2(\omega_q) \tag{3.63b}$$
$$F_3(\omega_q) = -2j\psi\omega_q e^{-j\omega_q 2\tau} e^{j\omega_q \epsilon} F^2(\omega_q) \tag{3.63c}$$
$$F_4(\omega_q) = -j\omega_q F(\omega_q). \tag{3.63d}$$

Equation (3.61) may be simplified further by using a matrix form. Let the vector of derivatives in (3.63), $\boldsymbol{\nabla F}$, be defined as

$$\boldsymbol{\nabla F} = [F_1(\omega_q), F_2(\omega_q), F_3(\omega_q), F_4(\omega_q)]^H. \tag{3.64}$$

Then, it can be seen that the Fisher information matrix can be expressed in matrix form as

$$\boldsymbol{J} = \frac{2}{T_o N_o} \sum_{q=-Q}^{Q} G(\omega_q)|D(\omega_q)|^2 \mathrm{Re}\left[\boldsymbol{\nabla F} \boldsymbol{\nabla F}^H\right]. \tag{3.65}$$

Furthermore, the term $|D(\omega_q)|^2$ may be simplified by using the ergodic assumptions of the symbols A_k in (2.37). The data dependent term then becomes

$$|D(\omega_q)|^2 = \sum_{n=0}^{N-1} \sum_{l=0}^{N-1} A_n A_l^* e^{-j\omega_q (n-l)T} \tag{3.66}$$
$$\simeq N P_{\mathrm{A}}, \tag{3.67}$$

where the approximation comes from the ergodicity in the autocorrelation assumption in (2.37b) and holds for N large enough. With this approximation, the Fisher information matrix finally becomes

$$\boldsymbol{J} \simeq \frac{2NP_{\mathrm{A}}}{T_o N_o} \sum_{q=-Q}^{Q} G(\omega_q) \mathrm{Re}\left[\boldsymbol{\nabla F} \boldsymbol{\nabla F}^H\right]. \tag{3.68}$$

By inverting the matrix, the Cramér-Rao bound for a particular estimate can be directly found using (3.12).

Unfortunately, the expression for $\boldsymbol{J}$ is quite complex and it is difficult to draw conclusions for the inter-parameter coupling. Nonetheless, it consists of an important piece of information for evaluating the performance of the estimate.

Chapter 4

Compensation Filter

In this Chapter, the design of the compensation filter is addressed. The continuous-time ideal compensation filter is first developed. It is shown that it consists of a weighted sum of delayed delta functions. Unfortunately, the delays are not necessarily multiples of the sampling period, making the implementation in discrete-time difficult. The filter design technique based on the channel parameters is presented followed by a detailed discussion on issues related to the realization of fractional delays. To close this Chapter, we comment on the design choices associated to the implementation of the compensation system, which consists of the parameter estimator, the filter design algorithm and the filter itself.

4.1 Continuous-Time System and Discrete-Time Equivalent

The discrete-time equivalent ideal compensation filter based on the ideal continuous-time filter is now derived. Recall from Chapter 3 in (3.59) that the composite channel frequency response may be expressed as

$$F(\omega) = \frac{e^{-j\omega\epsilon}}{1 - \psi e^{-j\omega 2\tau}}, \tag{4.1}$$

where ψ is the complex reflection coefficient, τ is the time delay between reflections and ϵ is a small synchronization offset. Notice that the effects of the demodulation and symbol synchronization have been incorporated in (4.1) as explained in Appendix A. The perfect or ideal inverse channel $F^{-1}(\omega)$ is easily obtained; by definition $F(\omega)F^{-1}(\omega) = 1$, thus

$$F^{-1}(\omega) = e^{j\omega\epsilon}(1 - \psi e^{-j\omega 2\tau}), \quad |\omega| < \frac{\pi}{T}. \tag{4.2}$$

The channel effects are bandlimited so that no aliasing occurs when sampling at half the symbol rate is performed. In practice, bandpass filters would be present at the radio receiver, which would limit the input bandwidth to make sure no aliasing occurs.

The realization of this inverse channel is illustrated in block diagram form in Fig. 4.1, where the input is taken directly from the matched filter and the output goes to the sampler (see Fig 2.6). It can be observed from this diagram that the two delays involved are not necessarily fraction of the sampling interval. Furthermore, the compensation filter is non-causal because of the term representing an advance in time, $e^{j\omega\epsilon}$. This is not a major issue, as extra delay is added to the system by the line-of-sight channel (see Fig. 2.4) and the equalizer.

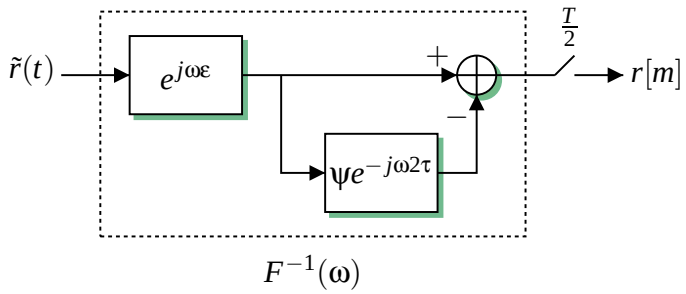

Fig. 4.1 Continuous-Time Compensation Filter

The channel inverse filter $F^{-1}(\omega)$ is to be implemented in digital hardware. As illustrated in Fig. 2.6, the discrete-time digital compensation filter $c[n]$, $n \in \{0, 1, \ldots, M-1\}$ where M represents the filter's length, is located after sampling by $T/2$. Consequently, the ideal inverse of Fig. 4.1 must be converted to the discrete-time domain to obtain the ideal inverse channel frequency response. Figure 4.1 illustrates the discrete-time compensation filter system. The input signal $\tilde{r}(t)$ is coming from the matched filters and the equalized samples are to be decimated by 2 and sent to the decision device.

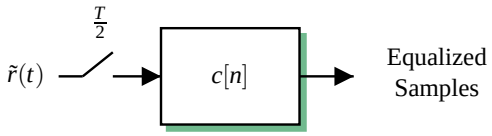

Fig. 4.2 Equivalent Digital Compensation Filter

To convert the ideal inverse channel frequency response to discrete-time form, it is assumed

that the system is bandlimited to at least half the sampling frequency so that no aliasing occurs. The main image of the equivalent discrete-time ideal channel inverse becomes, after sampling (4.2) with a sampling frequency of $2/T$ [26]:

$$\begin{aligned} C_{id}(\Omega) \equiv F^{-1}(\frac{2\Omega}{T}) &= e^{j\frac{2\Omega}{T}\epsilon}(1-\psi e^{-j\frac{4\Omega\tau}{T}}) \\ &= e^{j\frac{2\Omega}{T}\epsilon} - \psi e^{-j\frac{2\Omega}{T}(2\tau-\epsilon)}, \end{aligned} \tag{4.3}$$

where Ω represents the discrete-time frequency variable. Of course the discrete-time ideal inverse is periodic in frequency, and only the main image is considered here.

The filter design procedure consists of finding a set of filter coefficients $c[n]$, so that the discrete-time frequency response $C(\Omega)$ of that filter is close or ideally equal to the filter $C_{id}(\Omega)$, i.e.:

$$C(\Omega) = \sum_{n=0}^{M-1} c[n]e^{-j\Omega n} = C_{id}(\Omega). \tag{4.4}$$

The major obstacle to direct implementation of (4.4) is the presence of fractional delays in the system illustrated in Fig. 4.1. It can indeed be seen from (4.3) that two possibly noninteger delays are presents: a delay of $-\frac{2\epsilon}{T}$ and $\frac{2}{T}(2\tau-\epsilon)$. In discrete-time signal processing, only delays of a multiple of the sampling interval can be represented exactly. The problem therefore consists of finding a set of filter coefficients $d[n;t_0]$, where t_0 indicates the delay associated with the filter, that implements the ideal delay response

$$D_{id}(\Omega;t_0) = e^{-j\Omega t_0} \tag{4.5}$$

as closely as possible. Then by linearity, it can be seen from (4.3) that the compensation filter becomes

$$c[n] = d[n;-\frac{2\epsilon}{T}] - \psi d[n;\frac{2}{T}(2\tau-\epsilon)]. \tag{4.6}$$

4.2 Implementation of Noninteger Delay

In this section, the implementation of a fractional delay (FD) using a discrete-time digital FIR filter is discussed. Some general concepts are first introduced followed by a description of the least squares (LS) procedure for general weight functions. Some particular weight functions that are effective in the case of interest are then presented. Variable delay filters are finally discussed.

The noninteger delay filter design procedure should be simple enough so that it can be implemented on real-time hardware. It should ideally lead to short filters with good frequency responses. In general, for these types of filters to have the best frequency response for a given length, it is necessary to have the overall filter delay be half the filter's length [27]. For this to be the case, an extra integer-value delay must be added to the fractional delay, e.g. $t_0 + \lfloor \frac{M}{2} \rfloor$. For the remaining of this Chapter, it will be assumed that this requirement is satisfied.

The general FD problem consists of designing a discrete-time filter that implements as closely as possible the frequency response in (4.5). The difficulty is to have a constant magnitude and delay for a large bandwidth, with a finite length filter. Several methods exists for designing such filters [27], including the simple Lagrange interpolator, the general least squares approximation and the Farrow structure for variable delay filters.

Lagrange interpolators can be used for FD finite impulse response filter design. While they are very simple to implement, their bandwidth increases slowly with the number of coefficients and for filters with more than four taps as in the case of interest, it may be better to use a least squares approach. The least squares approach and the Farrow structure methods are discussed below.

4.2.1 Least Squares Design of Fractional Delay Filters

The least squares approach minimizes a user defined weighted squared error function. The error function is defined here as the difference between the frequency response of the designed filter $D(\Omega)$ and its desired or ideal response, $D_{id}(\Omega)$. The total squared error J can then be expressed as

$$J = \frac{1}{2\pi} \int_{-\pi}^{\pi} Q(\Omega) |D(\Omega) - D_{id}(\Omega)|^2 d\Omega, \tag{4.7}$$

where $Q(\Omega)$ is the real-valued weighting function, chosen by the designer. It is used to put more or less importance on the error at some specific frequencies.

It will be shown shortly that the optimal solution is obtained by solving a system of linear equations. If the weighting function is independent of the delay, then the matrix involved in the linear system solution will also be independent of the delay. It can therefore be inverted once off-line and put in memory for later use.

The desired response in (4.7) consists of the ideal delay (4.5) denoted here by $D_{id}(\Omega)$, where the reference to the delay t_0 is dropped for simplicity. The designed filter is denoted by $D(\Omega)$. To derive the minimum of (4.7) for this particular problem, important notation is first introduced.

Let $\boldsymbol{d}$ denote the vector of filter coefficients and $\boldsymbol{e}$ denote the vector of exponential functions of the Fourier transform, i.e:

$$\boldsymbol{d} = [d[0], d[1], \ldots, d[M-1]]^T, \tag{4.8}$$

$$\boldsymbol{e} = [1, e^{-j\Omega}, \ldots, e^{-j\Omega(M-1)}]^T. \tag{4.9}$$

Then the Fourier transform of the filter can now be expressed in a convenient vector product:

$$D(\Omega) = \sum_{n=0}^{M-1} d[n]e^{-j\Omega n} = \boldsymbol{d}^T\boldsymbol{e}. \tag{4.10}$$

This vector notation will allow the minimization of (4.7) to be expressed in a matrix form. Using this new notation and expanding the magnitude squared error in (4.7), the expression for the error J can be expressed as

$$J = \frac{1}{2\pi}\int_{-\pi}^{\pi} Q(\Omega)\left[\boldsymbol{d}^T\boldsymbol{e}\boldsymbol{e}^H\boldsymbol{d}^* - 2\text{Re}(e^{-j\Omega t_0}\boldsymbol{d}^T\boldsymbol{e}) + 1\right] d\Omega, \tag{4.11}$$

Noting that $\boldsymbol{e}$ is function of the integration variable Ω, the notation can be reduced further by introducing the matrix $\boldsymbol{P}$, the vector $\boldsymbol{p}$ and ξ_0 defined respectively as

$$\boldsymbol{P} = \frac{1}{2\pi}\int_{-\pi}^{\pi} Q(\Omega)\boldsymbol{e}\boldsymbol{e}^H d\Omega \tag{4.12}$$

$$\boldsymbol{p} = \frac{1}{2\pi}\int_{-\pi}^{\pi} Q(\Omega)e^{-j\Omega t_0}\boldsymbol{e}\, d\Omega \tag{4.13}$$

$$\xi_0 = \frac{1}{2\pi}\int_{-\pi}^{\pi} Q(\Omega)d\Omega. \tag{4.14}$$

Finally, the total squared error to be minimized is expressed in matrix form:

$$J = \boldsymbol{d}^T\boldsymbol{P}\boldsymbol{d}^* - 2\text{Re}[\boldsymbol{d}^T\boldsymbol{p}] + \xi_0, \tag{4.15}$$

where ξ_0 is independent of the filter's coefficients and will be nulled by the minimization.

To obtain filter coefficients that give the minimum least squared error, (4.15) is differentiated with respect to $\boldsymbol{d}$ and then the result is set to zero. Since both $\boldsymbol{d}$ and $\boldsymbol{p}$ are complex quantities, a complex gradient operator must be used for the minimization of (4.15). Using the results

from [28], the set of filter coefficients $\boldsymbol{d}$ that minimizes the squared error is given by

$$\boldsymbol{d} = \boldsymbol{P}^{-1}\boldsymbol{p}^{*}. \tag{4.16}$$

Provided that $Q(\Omega)$ is independent of the delay, $\boldsymbol{P}$ will also be independent of the delay and can be inverted off-line. The filter design then only involves computing $\boldsymbol{p}$ and applying (4.16).

The degree of complexity in the computation of $\boldsymbol{P}$ and $\boldsymbol{p}$ is highly influenced by the choice of weighting function. Here, three different possibilities for $Q(\Omega)$ are suggested and their respective properties are discussed.

Flat Weight

The first choice for $Q(\Omega)$ is the obvious constant function where the weight of the error is distributed uniformly across the entire spectrum:

$$Q_{\mathrm{F}}(\Omega) = 1. \tag{4.17}$$

The formulation for $\boldsymbol{P}$ and $\boldsymbol{p}$ for this case is very simple and it can be shown that element (k, l) of the matrix $\boldsymbol{P}$ and element k of the vector $\boldsymbol{p}$ are given respectively by [27]

$$P(k, l) = \mathrm{sinc}(k - l), \tag{4.18}$$

$$p(k) = \mathrm{sinc}(k - t_0). \tag{4.19}$$

Here it can be observed that matrix $\boldsymbol{P}$ is indeed independent from the delay t_0. Furthermore, since the sinc function is zero for all integer values of its argument except 0, i.e.:

$$\mathrm{sinc}(k) = \begin{cases} 1, & k = 0, \\ 0, & k \neq 0, \quad k \in \mathbb{Z} \end{cases} \tag{4.20}$$

the matrix $\boldsymbol{P}$ is in fact the identity matrix and the filter's coefficients are identical to the elements of $\boldsymbol{p}^{*}$. The coefficient are then exactly that of the truncated ideal response:

$$d(n) = \mathrm{sinc}(n - t_0), \quad n \in \{0, \ldots, M - 1\}. \tag{4.21}$$

Because of the sharp cut-off frequency (at $\Omega = \pm\pi$) and because the filter's time response must be truncated, it will suffer from Gibbs phenomenon. One way to minimize the effects of this is to use windowing [29]. However this will make the transition region wider and the choice of window does not follow any optimal criterion.

Bandlimited Weight

Sometimes, the signal to be delayed does not cover the entire bandwidth. In those situations, the error that lies outside the signal bandwidth is irrelevant to the overall performance. Therefore, a weight of zero for some "don't care" regions and one otherwise can be used.

Consider the case where the signal of interest is lowpass and limited in frequency to $\alpha\pi$, $(0 < \alpha \leq \pi)$. Then, a better choice for $Q(\Omega)$ is

$$Q_{\text{BL}}(\Omega) = \begin{cases} 1, & |\Omega| < \alpha\pi \\ 0, & \text{otherwise.} \end{cases} \tag{4.22}$$

It can be easily shown that element (k, l) of $\boldsymbol{P}$ and element k of $\boldsymbol{p}$ for this particular case are given respectively by

$$P(k, l) = \alpha\,\text{sinc}(\alpha(k - l)), \tag{4.23}$$

$$p(k) = \alpha\,\text{sinc}(\alpha(k - t_0)). \tag{4.24}$$

Again, $\boldsymbol{P}$ is independent of the delay but unlike the previous case, matrix $\boldsymbol{P}$ does not correspond to the identity matrix. This formulation of the error weight function should give better results than the previous one but will also suffer from Gibbs phenomenon because of the sharp transition. Once again, windowing can be used to attenuate this effect with consequences similar to those mentioned above.

Signal Power Spectral Density Weight

In some other situations, more information on the signal may be available. In particular, in situations where the power spectral density of the filter input signal is known, this information may be used for the weighting function. Of course, the PSD is application specific and cannot be generalized. Therefore, only the case of this particular application, where the filter input consists

of a series of randomly weighted raised cosines, will be considered.

The signal power spectral density may be expressed in frequency as the magnitude squared of the raised cosine frequency response in (2.19). Normalizing the result and converting it to discrete-time frequency (sampled at rate $T/2$), the power spectral density weight can be expressed as

$$Q_{\text{PSD}}(\Omega) = \begin{cases} 1, & 0 \leq |\Omega| < \frac{1-\beta}{2}\pi \\ \frac{1}{4}\left\{1 + \cos(\frac{1}{\beta}(|\Omega| - \frac{1-\beta}{2}\pi))\right\}^2, & \frac{1-\beta}{2}\pi \leq |\Omega| \leq \frac{1-\beta}{2}\pi \\ 0, & \frac{1+\beta}{2}\pi < |\Omega| < \pi. \end{cases} \tag{4.25}$$

Using $Q_{\text{PSD}}(\Omega)$ as weighting function in (4.12) and (4.13) leads to long and complex equations, which however may be obtained easily through the use of a symbolic computations software (e.g. Waterloo Maple). Because the transition between the two bands is smoothed by the raised cosine in (4.25), the importance of the Gibbs phenomenon will depend on the roll-off factor β. In the radio unit under investigation, $\beta = 1/3$, which means that the transition band is relatively large and Gibbs phenomenon effects will be practically inexistent. This results in a smoother frequency response which follows closely the desired response in the signal's bandwidth.

4.2.2 Example of Inverse Filter

Using the results of previous sections, a compensation filter for an hypothetical channel is now designed using different weight functions. In particular, the differences in frequency responses between a filter designed using a bandlimited weight $Q_{\text{BL}}(\Omega)$ in (4.22) and power spectral density weight $Q_{\text{PSD}}(\Omega)$ in (4.25) will be compared.

Consider a channel as defined in eq. (4.1), with parameters $|\psi| = 0.1$,$\measuredangle\psi = \pi/6$, $\tau = 0.25T$ and $\epsilon = 0.0249T$. The pulse shape consists of a raised cosine with rolloff factor $\beta = 1/3$; the signal's bandwidth thus extends in frequency up to $\pm\frac{2\pi}{3}$.

The frequency response of the designed filters are illustrated in Fig. 4.3, where the ideal compensation filter frequency response is denoted by $C_{id}(\Omega)$ and the compensation filters designed using the bandlimited ($\alpha = 2/3$) and power spectral density weights are denoted by $C_{\text{BL}}(\Omega)$ and $C_{\text{PSD}}(\Omega)$ respectively.

It can be observed from Fig. 4.3 that the filter designed using the power spectral density weighting function follows the ideal frequency response very closely in the signal's bandwidth, as indicated by the vertical dashed lines, i.e. from $-2\pi/3$ to $2\pi/3$. The filter designed using the limited bandwidth weighting function on the other hand is close from the ideal response only in a

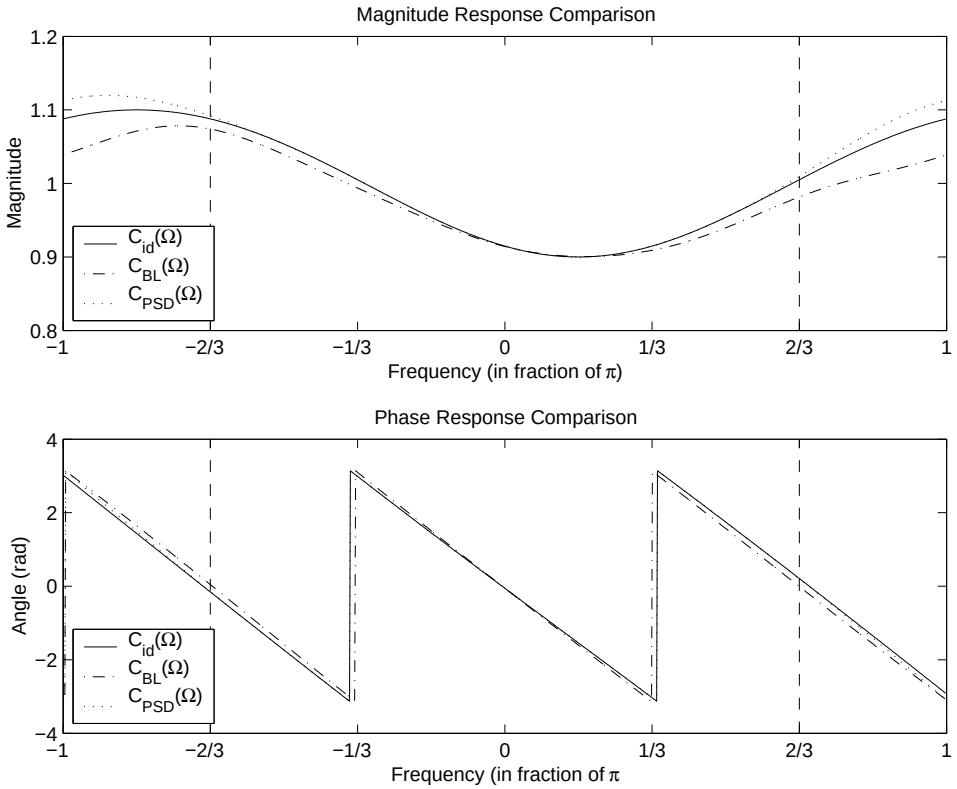

Fig. 4.3 Compensation Filter Frequency Response Comparison

close neighborhood of the origin and deviates from the ideal response with increasing frequency.

4.2.3 Variable Delay Filters

The problem with the previous delay filter design techniques is that each time the delay changes, a new vector $\boldsymbol{p}$ must be obtained and then (4.16) must be applied to get the new filter coefficients. This may be too computationally intensive for applications where the delay changes continuously. In those situations, Farrow [30] structure may be used.

The basic concept of a Farrow structure is to obtain a set of coefficients for a variable-delay filter from the interpolation of a set of fixed-delay filters. The fixed-delay filters are designed off-line using some filter design method such as above. The structure uses polynomial interpolation in the variable delay t_0 that controls the weight on each set of filter coefficients. Unfortunately, this adds a level of approximation to the filter and may not give optimal results. In any cases, the implementation details of Farrow structures will not be discussed in more details here and the interested reader is encouraged to consult [30, 29].

In this work, the focus in put on the design of the compensation filter using the least squares approach with the power spectral density weight function. This method is straightforward and produces reliable filters. The compensation system introduces a first level of approximation when estimating the parameters. For this reason, to minimize the number of approximation levels, the least squares approach is chosen in preference of the Farrow structure.

4.3 Block versus Iterative

The design of a compensation filter using the least squares approach takes a certain amount of computations. First, the vector $\boldsymbol{p}$ needs to be computed and then multiplied by the inverted $\boldsymbol{P}$ matrix. All of these operations must be performed on-line. Unless a Farrow structure is utilized, updating the compensation filter at every sample is impracticable. In this section, the design issues related to the implementation of the compensation system for this specific application are discussed.

For the implementation of the parameter estimator discussed in Chapter 3, the designer has the choice of using a block estimator as illustrated in Fig. 3.4 or an iterative estimator as in Fig. 3.5. For the block estimator case, the estimated parameters are only available after the estimation procedure is completed. The procedure requires N samples to be buffered first and then requires

a certain time to converge to the final solution. Most optimization algorithms are not guaranteed to converge in a prescribed number of iterations. Unless the optimization algorithm is modified in a way to limit the convergence time, which may limit the performance of the estimates, the time required to obtain a set of estimate is unknown. Therefore, the time between filter coefficients updates is also unknown.

By using the iterative estimation approach however, the designer has access to a new estimate every sample, without risking estimate performance degradation. Since the compensation filter design in itself takes some time, it may not be practical to obtain a new set of equalizer coefficients every sample. Depending on the hardware available and the choice of filter design method, the designer has to decide on how much time (in number of samples) there will be between each coefficient update. The process is illustrated in Fig. 4.4, where N represents the number of samples between each coefficient update.

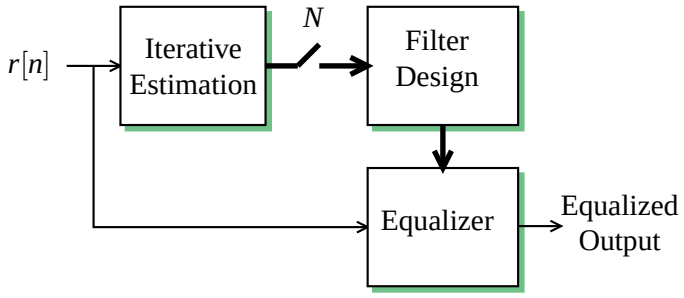

Fig. 4.4 Iterative Compensation System

The designer has to decide, based on the hardware available and on the precision requirements, which method is more appropriate to use and how much delay is needed between each coefficients update. In addition, the more samples are used in the estimation, the better the precision of the estimates is. However, it also means a longer delay between coefficients update for the block structure. Similarly for the iterative approach, choosing a small step-size will lead to better estimates, but will take longer to converge.

In this work, the iterative estimator is used in conjunction with the least squares filter design method with the power spectral density weight. Every sample, an estimate of the parameters is available. However, only every thousand samples $(N = 1000)$ does a new filter is designed and loaded into the channel equalizer. Results, showing the performance of this compensation system compared to other adaptive equalization techniques, are illustrated in Chapter 5.

Chapter 5

Results

This chapter exposes the results related to the different aspects of this work. In particular, the iterative estimator, the block estimator and its associated Cramér-Rao bound, and the proposed compensation system are considered.

To begin this Chapter, the methodological aspects are discussed, with a description of the simulation procedures. The results related to the parameter estimation Chapter are then presented. The convergence plots of the joint iterative estimator algorithm are shown along with a comparison of the variance of the joint block ML estimator with the corresponding Cramér-Rao lower bound. Finally, the implementation of the proposed compensation system is compared with some current adaptive channel equalization techniques.

5.1 Methodology

The results were all obtained through simulations of the communication system. The simulation model is based on the theoretical lowpass model developed in Chapter 2. It was implemented in software using the scripting capabilities of mathematical software tool *MATLAB*. Some functions were implemented in *C* to improve the speed of the calculations.

The simulation model used is illustrated in Fig. 2.6. The “Binary Source” and “MAP” blocks shown in the diagram are implemented in the simulator by using a uniform random generator that generates the sequence of complex symbols from set of 32 possibilities (QAM-32) in the constellation of Fig. 2.7. The sequence is then upsampled and convolved with the pulse shaping function at a new sampling rate of ten times the symbol rate. This oversampling allows the simulator to have a wider range of possible reflection delays. The pulse shape consists of the raised

cosine expressed in (2.21), oversampled and truncated to a length equivalent to twelve symbols on each side of the main peak. Since the raised cosine decreases in magnitude proportionally to $1/t^3$, it is reasonable to assume that twelve symbols is long enough to accurately represent the system. The channel is implemented using an ordinary IIR structure. After the channel, the signal is decimated by five, to a rate of twice the symbol rate. This is the rate at which the equalizer operates.

The noise is generated using a normally-distributed random number generator, independently on each quadrature. It is then filtered by a half-spaced square root raised cosine, simulating the effects of the matched filter in Fig. 2.6.

To objectively compare different algorithms, the equalizer's length was fixed to eight complex taps. After the equalizer, the signal is downsampled by two to match the symbol rate and the decision device then simply selects the symbol that is the closest to the equalized sample.

5.2 Parameter Estimation Results

In this section, the results obtained for the parameter estimation part of the work are presented. Two different experiments were performed for this part. First, the convergence properties of the iterative estimator of section 3.3.2 at two different signal-to-noise ratios are shown. Second, the variance of the joint block ML estimator is compared with the Cramér-Rao lower bound.

5.2.1 Iterative Estimator

The iterative estimator presented in Chapter 3 requires the computation of the gradient of the log-likelihood function. To do so, it needs to compute (3.53), which consists of a double sum over an infinite number of elements. The inner sum, i.e. the sum over k in (3.52) and (3.54), must be limited to a number of symbols around the origin at time n.

Since the pulse function is limited in length by twelve times the symbol duration, only the adjacent twelve symbols on each side of a given sample will affect it. Consequently, the sums in (3.52) and (3.54) are also limited to twelve symbols on each side of the current time index n. The outer sum, i.e the sum over l in (3.53), is the sum over all reflections and it is limited to three reflections (i.e. $L = 3$) for this particular experiment.

Computation of (3.52) and (3.54) requires the knowledge of the transmitted symbols. In this experiment, it is assumed that the probability of error is small for high signal-to-noise ratio and

that the exact values of the symbols are available.

The adaptation curves for the four parameters $|\psi|$, $\measuredangle\psi$, τ and ϵ are shown in Fig. 5.1. The parameters were chosen to have physically plausible values, with $|\psi| = 0.1$, $\measuredangle\psi = 0.25$(rad), $\tau = 0.5T$, and $\epsilon = 0.0264T$ and their respective step-sizes were $\mu^1 = 0.0001$, $\mu^2 = 0.004$, $\mu^3 = 0.0005$ and $\mu^4 = 0.0001$. The step-sizes were chosen heuristically to have good convergence properties. Note that the parameters are inter-dependent and coupling exists in the step-sizes, making the selection of step-size difficult.

The figure shows the values of the estimate for each parameter with respect to time, measured in half-spaced symbols. For each parameter, two curves are shown; the first (solid) curve shows the value of the estimate at a signal-to-noise ratio of $E_b/N_o = 20dB$ and the other shows the estimate at very high SNR, i.e. $E_b/N_o = 120dB$. The dotted line indicates the real value of the parameter. All of the estimates converge to their respective parameter value, confirming that the number of reflections ($L = 3$) is large enough to obtain a good approximation to the infinite sum in (3.53). It can also be observed that the convergence rate at low SNR is similar to the high SNR case but the fluctuations in the estimate are larger. Consequently, if for a given convergence rate the level of the noise is such that the estimates are too noisy to be used, then the only way to obtain better estimates is to have a smaller step-size, which ultimately increases the convergence time.

The symbols A_k are assumed to be known at the receiver with a low probability of error. It is nonetheless important to investigate the effects of a decision error on the algorithm as it may occur once in a while. To do so, the same experiment as above is performed with an error in one symbol decision artificially introduced. When doing this, no effects on the adaptation curves could be perceived. The adaptation step-sizes chosen are too small for a single error to cause disturbance. Note that the erroneous symbol was chosen such that it is adjacent in the constellation to the real transmitted symbol. That way, it represents more closely what would be observed in practice in a low probability of error environment.

5.2.2 Cramér-Rao Bound

The joint block ML estimator discussed in Chapter 3 was implemented in *MATLAB*. The optimization routine for non-linear constrained minimization, based on a Sequential Quadratic Programming (SQP) method [23], was used in this experiment to obtain the estimates. The experiment was repeated one hundred times using the same parameters as those selected in the previous

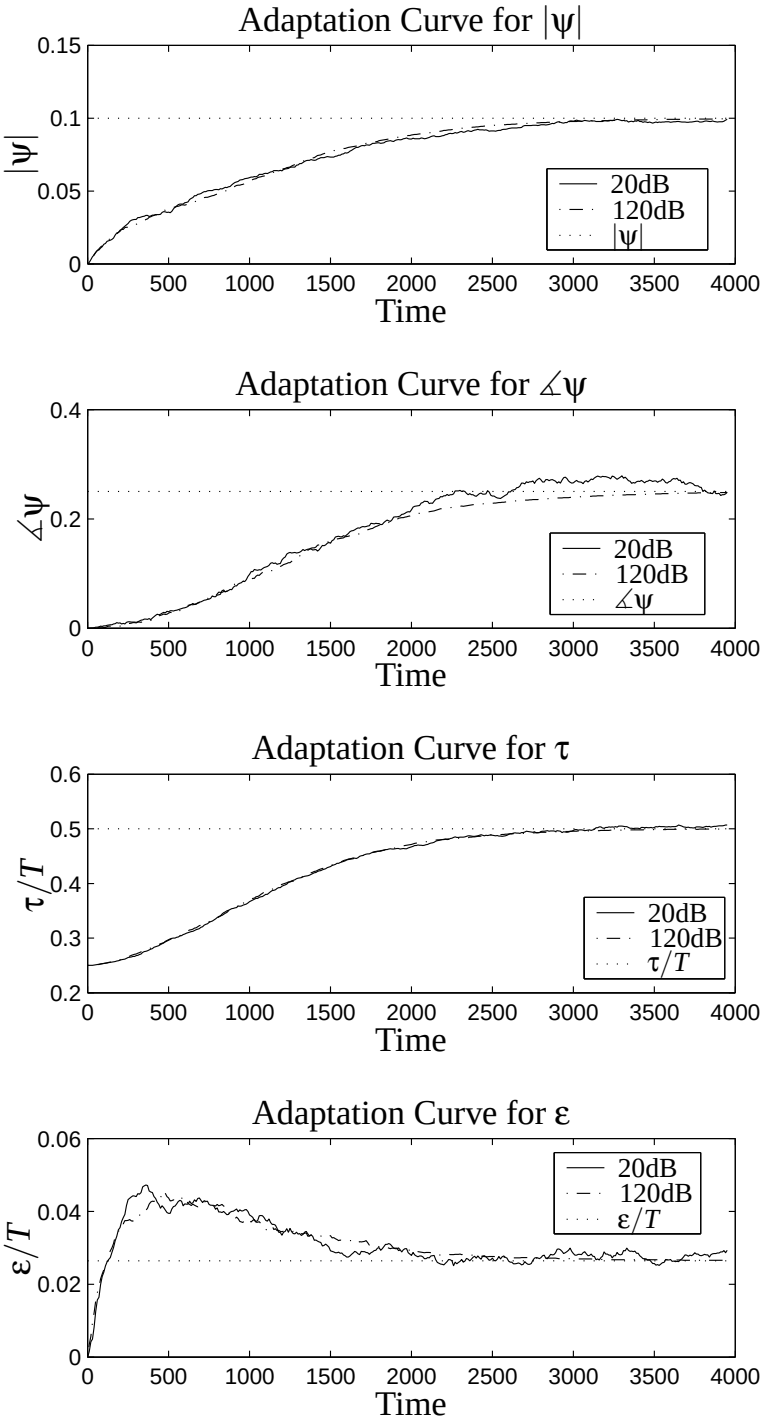

Fig. 5.1 Adaptation Curves for the Iterative Estimator

experiment and the variance of the estimates obtained was computed.

The objective is to compare the variance obtained to the Cramér-Rao bound, in (3.12) through the inversion of the Fisher information matrix in (3.68).

The CRB requires non-biased estimates. This is a problem if an infinite number of channel reflections must be considered. Therefore, to guarantee an exactly non-biased estimate even at very high SNRs, the number of reflections was chosen to be limited to two in the channel. That way, the channel becomes FIR and $u[n]$ in (3.37) with the number of reflections also limited to (two) exactly represents the received signal, without noise. Therefore the estimate obtained using the procedure suggested is un-biased and the Cramér-Rao lower bound can be applied and compared to the experimental data.

The results of this experiment for the four parameters are shown in Fig. 5.2 and 5.3 for a block size of $N = 1000$ and $N = 200$, respectively. For the larger block size in Fig. 5.2, the solid line corresponds to the Cramér-Rao lower bound and the dotted lines represents the experimental data. This experiment was performed using symbol-spaced samples, i.e. sampling interval T, and half-symbol spaced samples, i.e. sampling interval $T/2$. The data points indicated by a circle "$\circ$" and by a diamond "$\diamond$" represent the experiments with sampling interval of T and $T/2$ respectively.

In Fig. 5.3, blocks of $N = 200$ samples are used the experiment only considers symbol-spaced samples. The experimental data points are indicated by a circle, while the theoretical bound is indicated by the straight line with the squares as data markers.

First, consider the data set corresponding to the experiment which used a block size of $N = 1000$ and symbol-spaced samples (T). It can be observed from Fig. 5.2 that the experimental data has the same slope than the CRB, for all parameters. Interestingly, it can also be observed that the distance between the bound and the experimental data varies from parameter to parameter.

In particular, it can be seen that the distance between the variance of ϵ, a pure delay, and the corresponding CRB is larger than for the other estimates. For pure delay estimation in white noise, the CRB, σ^2_{D}, may be given by [31]

$$\sigma^2_{\mathrm{D}} = \frac{K}{T_{\mathrm{o}}(f_2^3 - f_1^3)}, \tag{5.1}$$

where K is a constant that depends on the signal-to-noise ratio, T_{o} is observation time, f_1 and f_2 are the lower and upper limit on the signal's bandwidth respectively. Since sampling at the symbol rate implies (using normalized frequencies) $f_1 = 0$ and $f_2 = 1/2$ and since the system's bandwidth corresponds to $f_2' = 2/3$, then it is expected that the CRB when using symbol-spaced

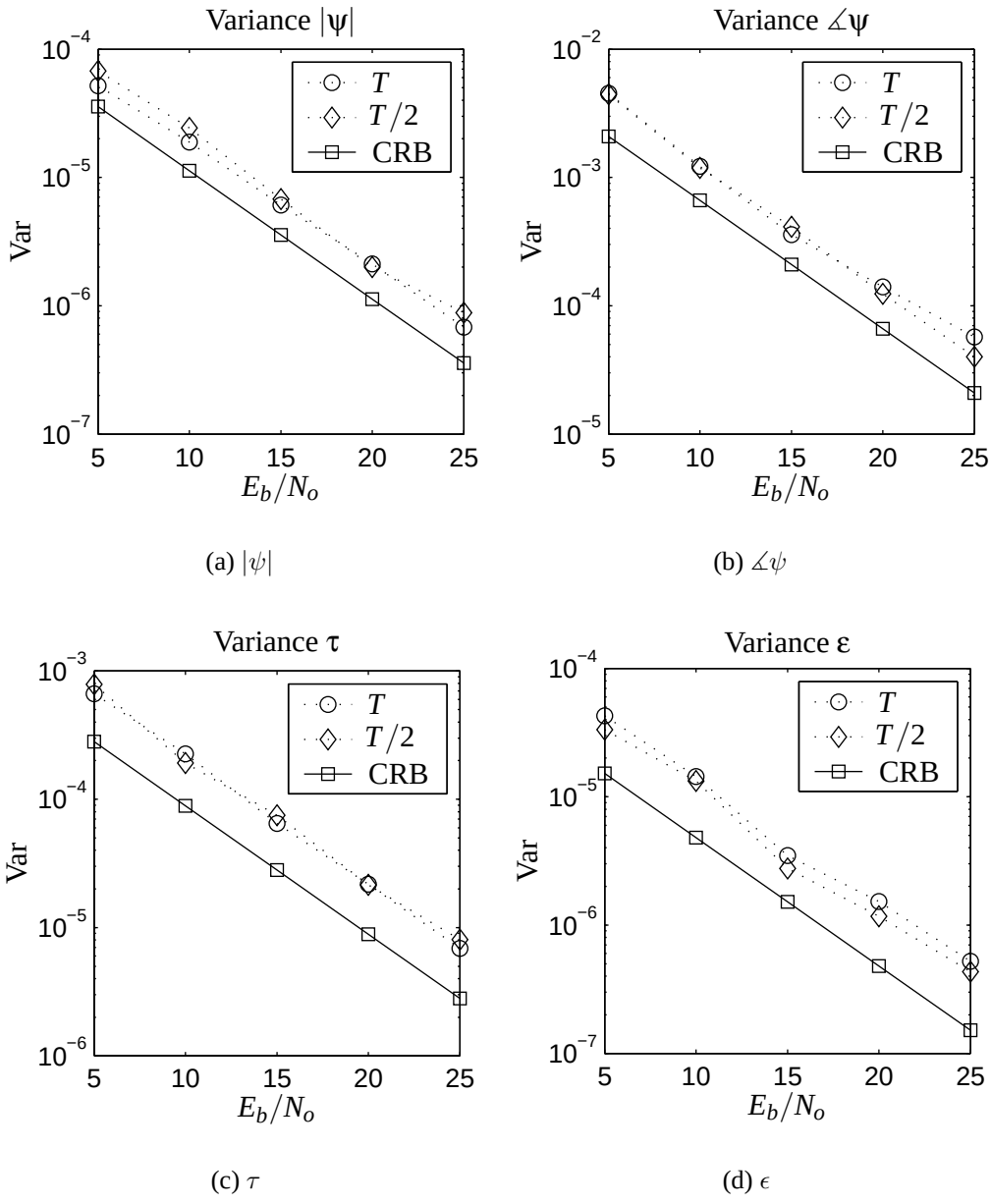

(a) $|\psi|$ (b) $\angle\psi$

(c) τ (d) ϵ

Fig. 5.2 Estimate Variance vs Cramér-Rao Bound for Block of 1000 Samples

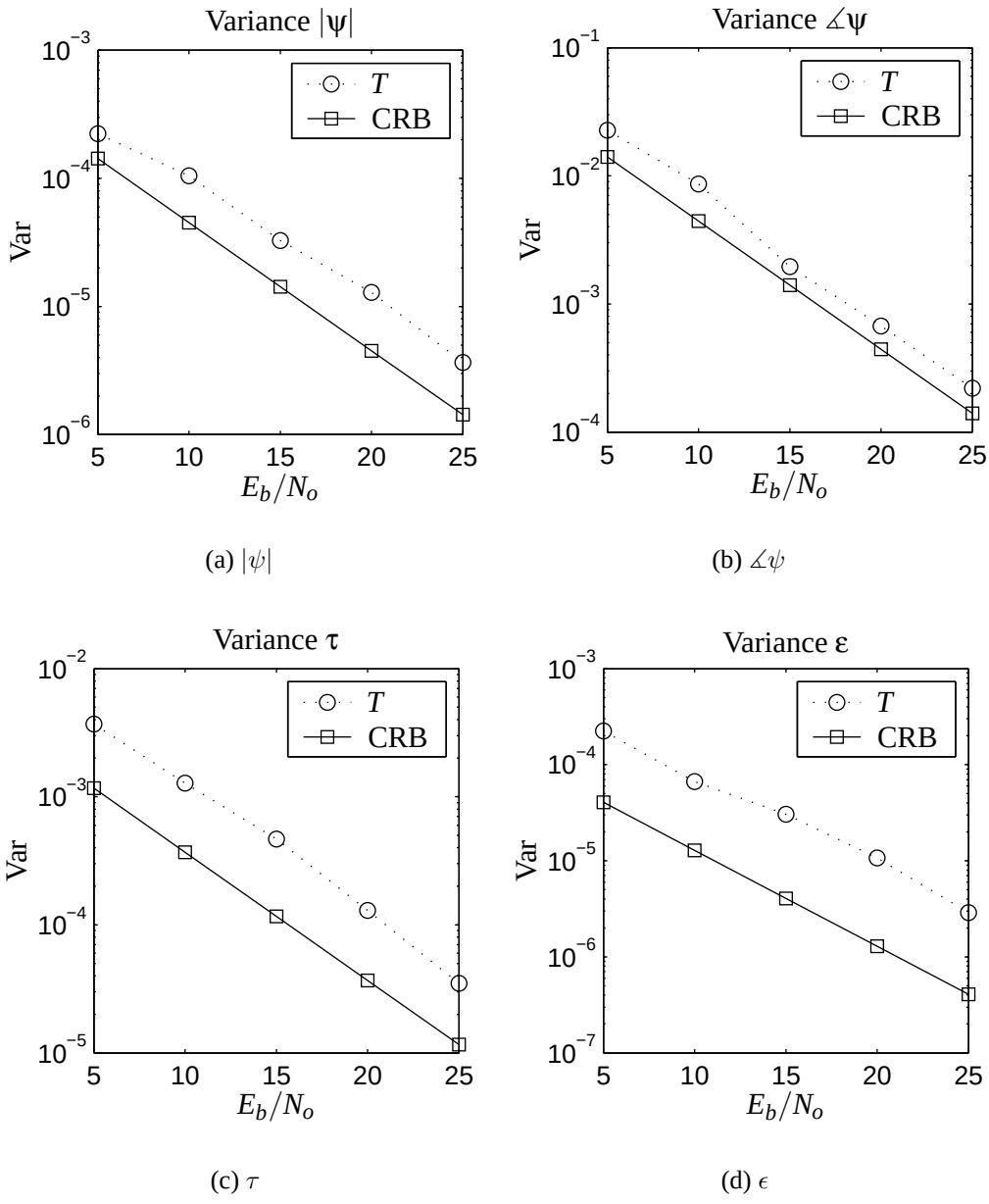

(a) $|\psi|$ (b) $\angle\psi$

(c) τ (d) ϵ

Fig. 5.3 Estimate Variance vs Cramér-Rao Bound for Block of 200 Samples

samples is approximately $\frac{(1/2)^3}{(2/3)^3} \approx 2.4$ times the CRB when using the full signal's bandwidth.

Hence in this case, the CRB curve in Fig. 5.2(d) would be 2.4 times higher than the current one, bringing the CRB closer to the experimental data. The average distance between the CRB and the variance of the estimate obtained using symbol-spaced samples is approximately 2.9. The difference may be explained by the modelling; the estimation performed in this experiment is joint and the variance of ϵ also depends on the other parameters whereas (5.1) does not take the joint estimation into account.

The variance of the estimate when using half-symbol spaced samples ($T/2$) is not significantly closer to the bound than the other case (T) and is even further for the variance of $\|\psi|$. This may be explain from the lack of pre-whitening filter for the $T/2$ case; (5.1) only holds for white Gaussian signals. Therefore, without the pre-whitening filter, the power of the signal's higher frequencies remains negligible and nothing is gained.

The variance of the estimate for smaller observation time tends to be further from the CRB than for larger observation time as can be observed from Fig. 5.3. For instance, the ratio of the average difference between the variance of the estimate and the CRB for $N = 200$ and $N = 1000$ is approximately 6. So for an observation time five times larger, the average difference between the variance and the bound decreases approximately by a factor of 6. This trend is expected from a ML estimator; as the observation time increases, the variance of the estimate tends to the Cramér-Rao lower bound [9].

5.3 Compensation System Comparison

In this section, the iterative estimation procedure of Chapter 3 is combined with the filter design techniques discussed in Chapter 4 to obtain a full compensation system and investigate its performances. To do so, the mean squared error (MSE) between the symbols sent (A_k) and the equalized samples at the input of the decision device is computed for each compensation system, as illustrated in Fig. 5.4. Then the MSE from the different compensation systems are compared.

As shown in Fig. 5.4, the mean square error between the exact symbol and the equalized samples is computed over N symbols. Smaller MSE at the input of the decision device indicates a smaller symbol error rate. A better measure would be to compare the symbol error rate directly (i.e the number of $\hat{A}_{k-d} \neq A_{k-d}$ over the number of symbol sent), however this is not practical because of the extremely low probability of error (recall that the BER for this radio unit is approximately 10^{-8}). Hence, the comparision of MSE is the preferred method in this work.

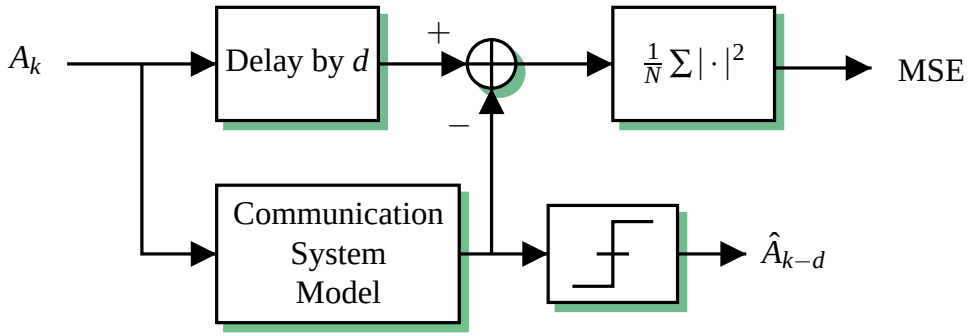

Fig. 5.4 Mean Square Error Computation

Compared Systems

In this comparative study, three different compensation systems are considered. The first compensation system, used in some existing data radio systems, consists of a bank of fixed FIR filters from which a filter is selected to perform the equalization for each block of duration 4096 samples. In this experiment, a set of seven FIR filters are considered. The first filter is the all-pass filter and the other six are designed for a fixed $|\psi|$, τ and ϵ, and six different values of $\measuredangle\psi$, uniformly distributed between $(-\pi, \pi]$. For every block of 4096 samples, one filter is selected as being the "best" filter, and its output is routed to the decision device. It is chosen according to its mean squared error (MSE), measured between the symbol sent (or its estimate) and the equalized output, during the previous block.

The MSE for the best filter is computed along with the MSE for the other filters, one at a time, alternating once per symbol duration during the entire block of data. At the end of a block, the filter with the lowest mean squared error is selected as the best filter and is used for equalization of the following block. This system will be referred to as "FBF" for fixed bank of filters.

The next system used in the comparison consists of an adaptive channel equalizer that uses the normalized LMS (NLMS) algorithm [3]. For this experiment, a normalized step-size of $\tilde{\mu} = 0.3$ was used for illustrative purposes. This specific value was chosen to have fast convergence and a relatively small excess error.

The compensation system that is utilized here for the comparison is the iterative compensation system illustrated in Fig. 4.4, where $N = 1000$. The iterative parameter estimator had step-sizes $\mu^1 = 0.0001$, $\mu^2 = 0.01$, $\mu^3 = 0.002$ and $\mu^4 = 0.001$. The compensation system estimates the parameters iteratively and once every $N = 1000$ samples, the parameters are used to design a

new compensation filter (equalizer). The filter is designed using a least squares approach with the signal power spectral density as error weighting function, as described in Chapter 4.

MSE Comparison Results

The simulations were performed at a signal-to-noise ratio of $E_b/N_o = 20dB$ and repeated over one hundreds different channels. The channel parameters were uniformly distributed over the range $[0, 0.2]$ for $|\psi|$, $(-\pi, \pi]$ for $\measuredangle\psi$, $[0.25, 0.75]$ for τ and $[-0.025, 0.025]$ for ϵ. Figure 5.5 shows the averaged MSE over the hundred channels for the different compensations algorithms.

The solid line at the top shows the MSE of the FBF system described above. The algorithm is initialized to the all-pass filter and changes filter after 4096 samples to the "best" filter for the previous block. Since the filters in the bank were designed for a fixed channel, i.e. for $|\psi| = 0.1$, $\tau = 0.25T$ and $\epsilon = 0$, it is expected that it does not perform well over the number of randomly generated channels.

The dashed curve shows the performance of the proposed compensation system, labelled "CS" for *Compensation System*. As the channel estimates converge to their respective values, the channel equalizer designed on-line gets closer and closer to its ideal form. For all practical purposes, it can be seen from Fig. 5.5 that after approximately six thousands samples, the estimates are close enough to their actual values for the compensation filter to have converge to its ideal response, lowering the MSE almost to the effective noise level, σ^2, indicated by the dotted line labeled "Noise" at the bottom.

The "dash-dot" line on the plot shows the MSE obtained using the NLMS algorithm. As it can be observed, the NLMS converges extremely quickly to its minimum. However because of the misadjustment in the LMS algorithm, it does not reach the minimum attainable MSE, σ^2. Note that a smaller step-size would results in a smaller excess mean square error and would get close to the noise level.

The compensation system can therefore achieve a MSE in the order of what the NLMS algorithm can achieve. However the new system has a level of complexity much higher than the normalized LMS algorithm. A quick analysis of Algorithm 3.1 shows that for each sample, the number of operation necessary to obtain a set of estimates is approximately $4(L+1) + 2(2K+1)(L+1)$, where L is the number of reflections taken into account in (3.53) and K is the number of symbols considered in (3.52) and (3.54). Thus, if we consider the filtering operation with a filter length of L_f, the total complexity for every sample for the new compensation system be-

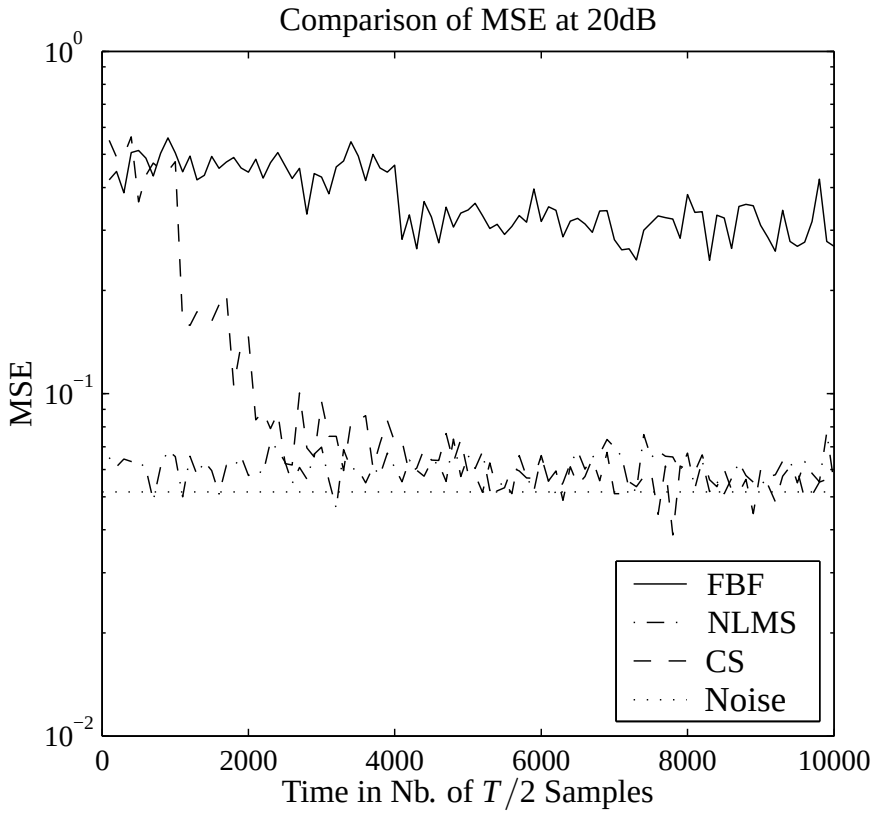

Fig. 5.5 Mean Squared Error Comparison

comes $L_f + 4(L+1) + 2(2K+1)(L+1)$ plus some overhead, whereas the level of complexity of the NLMS algorithm is in the order of $2L_f$ plus overhead and for the FBF algorithm it is $2L_f + 1$ plus overhead.

The proposed compensation system can therefore be advantageous in situations where the length of the filter is very long. In fact, the NLMS algorithm can be seen as a parameter estimator where the parameters are the filter's coefficients. For a complex filter of length L_f, there are $2L_f$ parameters to estimate whereas in this application, the number of channel parameters is only $M = 4$. Therefore for very long filters, i.e. $L_f \gg M$, it may be more appropriate to use the proposed compensation system.

Chapter 6

Conclusion

This work considered the estimation of transmission line parameters for digital equalization. It focused on a specific military high capacity line-of-sight radio system. The particular application of this radio is such that reflections on the cable between the antenna and radio receiver are inevitable, creating ISI at the receiver. The equalization procedure proposed to compensate for the ISI is performed in two steps. First, the transmission line parameters are estimated, using a probability model derived from the physics of the problem. Then, a compensation filter is designed (on-line) to equalize the distortion.

This Chapter will present a summary of the work followed by some suggestions on appropriate future work.

6.1 Summary of Work

Aforementioned, this thesis considers a particular communication system, designed and manufactured for the military. It is a general data radio used by the military during deployment. It is usually positioned in a communication vehicle, and requires a small installation time since it is subject to frequent location changes.

This radio unit creates high reliability links, compatible with *ATM* and can operate over a very wide range of carrier frequencies over two distinct bands. Its main performance degradation however, comes from the ISI caused by the reflections on the cable, between the antenna and the radio receiver. Those reflections exists because the installation requirements are such that tuning the antenna-cable-connection cannot be performed manually, causing an impedance mismatch.

The electrical properties of the transmission line system were analyzed in this work to obtain

a model for the received signal. The model uses four parameters to completely determine the effects of the transmission line reflections, or channel. The four parameters include the reflection coefficient ψ, a complex quantity with a magnitude $|\psi|$ and a phase $\measuredangle\psi$, the delay between reflections τ and the synchronization offset ϵ. The latter is indirectly caused by the channel; the received signal distortion will make the symbol synchronizer lock slightly offset with respect to the middle of the symbol.

Point estimation was used to estimate the parameters, based on the received signal. The maximum likelihood (ML) estimator was first derived using a Fourier series expansion of the received signal. Then, a more practicable approximate ML estimator that uses discrete-time samples has been proposed. The approximate ML estimator uses non-linear optimization procedures to minimize a cost function, closely related to its Fourier series ML estimator counterpart. To model the radio unit under conisderation accurately, the pre-whitening filter is neglected in the approximate ML estimator. In addition, an iterative estimator was presented. It is loosely based on the steepest descent technique. The iterative estimator may be more practical to use in real-time applications. Finally, the Cramér-Rao lower bound for the variance of the estimate was derived.

The estimated parameters are used to design a compensation filter. It was shown that the compensation filter can be expressed in the time-domain as a sum of two weighted delayed delta function. Unfortunately, the delays are not necessarily an integer number of sampling interval. Therefore, only an approximate filter may be designed. A method for designing fractional delay (FD) based on the least squares approach is suggested. The method weights the error in the frequency domain with the power spectral density of the transmitted signal. This way, the weight on the error is of lesser importance at the frequencies where the signal energy is low. The frequency response of the designed compensation filter follows closely the ideal inverse channel frequency response in the signal's bandwidth.

Convergence curves for the iterative parameter estimator were shown. The parameter estimates converge steadily to their actual values at the same rate for different SNRs, for a given step-size. When the step-size is small enough, the effects of an error in the symbol decision does not affect the estimates. The variance of the estimate obtained using a block ML estimator were compared to their respective CRB. It is shown that the variances are close to the bound except for the variance of the delay estimation, where it is slightly further from the bound than the other cases. It is advanced that the absence of a pre-whitening filter and the bandwidth limitation of the observation signal affect the reliability of the estimate. Finally, the full compensation system, incorporating the iterative estimator and the filter design, is compared to other channel equaliza-

tion techniques. The proposed method is shown to perform better than some sub-optimal channel equalization techniques currently used in the industry. The mean squared error of the proposed method approaches the power of the noise (minimum limit), as the estimates becomes closer to their actual values.

6.2 Future Work

This thesis focused on a particular practical problem proposed by the industry. As such, the future work suggested here involves both theoretical and practical aspects.

In terms of the theoretical future work, the issue of the automatic gain controllers should be addressed. The model developed ignores the possible gain variations in the received signal caused by the automatic gain controllers in reaction to the distortion and noise. A model for the gain variation should be developed. It should not be too difficult to incorporate a gain compensation system since the automatic gain can be predicted from the channel parameters and the noise power.

The iterative algorithm proposed was developed using fixed step-sizes. The convergence and stability of the algorithm could be improved by using an adaptive step-size mechanism. Ideally, the step-sizes should first be larger so that the convergence is rapid at the beginning. Then, when the estimates have converged, the step-sizes should be smaller to "fine tune" the estimates. A search in the general adaptive filtering literature for similar step-size control algorithms should be a good starting point. The iterative algorithm could also be modified to use the proposed bounds on the parameters. Finally, another interesting future work direction is to study the relationship between the Cramér-Rao bound and the iterative algorithm. In particular, it would be interesting to find a relation between the convergence time, the step-size and the steady-state variance of the estimate for the iterative algorithm.

The proposed compensation system relies heavily on the exactitude of the mathematical model developed for the channel. An important aspect of future work would be to validate the mathematical model using measured data. Ideally, those measurements should be made on a real system, to represent as closely as possible the real operating conditions. The algorithm should also be tested using real data.

The compensation system proposed is likely to be implemented in fixed point arithmetic. Therefore, issues regarding fixed point implementation should be addressed. In particular, the effects of limited numerical precision on the parameter estimation algorithm should be studied.

Study of the fixed point implementation will also help to determine the necessary hardware for the compensation system realization.

Appendix A

Lowpass Equivalent Communication Model Derivation

In this appendix, the lowpass equivalent communication system of Fig. 2.4 is fully derived. The latter makes abstraction of the modulation and is therefore mathematically easier to work with.

First, the lowpass equivalent of the transmitted signal is developed, then the channel and noise lowpass equivalent are derived. Finally, the matched filter and sampling are integrated to obtain an expression for the fractionally sampled signal at the input of the equalizer.

Transmitted Signal

The QAM signal sent by the transmitter (after pulse shaping by $p(t)$) is defined by

$$s(t) = \sum_{k=-\infty}^{\infty} A_{Ik} p(t - kT) \cos(\omega_c t) - A_{Qk} p(t - kT) \sin(\omega_c t) \tag{A.1}$$

where A_{Ik} and A_{Qk} are the in-phase and quadrature components of the symbol at time k respectively and T is the symbol duration. Since (A.1) is already in canonical form (see 2.27), its lowpass equivalent can be directly obtained:

$$\tilde{s}(t) = \sum_{k=-\infty}^{\infty} A_k p(t - kT), \tag{A.2}$$

where $A_k = A_{Ik} + jA_{Qk}$.

Channel

The channel's frequency response in equation (2.18) is not passband as it covers the entire frequency range. It is therefore assumed that the radio-receiver has a bandpass filter at its input. The latter is assumed to be

$$\Pi(\omega) = \begin{cases} 1, & \omega_c - W < |\omega| < \omega_c + W \\ 0, & \text{elsewhere}, \end{cases} \tag{A.3}$$

where ω_c is the center frequency of the filter and $2W$ is its total (bandpass) bandwidth. With this filter in place, it is not difficult to show that the lowpass equivalent channel response becomes

$$\tilde{H}(\omega) = 2e^{-j(\omega+\omega_c)\tau}\left(\frac{\phi}{1-\psi e^{-j(\omega+\omega_c)2\tau}}\right), \quad |\omega| < W \tag{A.4}$$

and $\tilde{H}(\omega) = 0$ otherwise. If the lowpass excitation $g(t)$ is band-limited to $|\omega| < W$, it is possible to make abstraction of the frequency limitation $|\omega| < W$ in (A.4) and express its time domain equivalent as

$$\begin{aligned} \tilde{h}(t) &= 2\phi[\delta(t-\tau) + \psi\delta(t-3\tau) + \psi^2\delta(t-5\tau) + \ldots] \\ &= 2\phi\sum_{l=0}^{\infty}\psi^l\delta(t-(2l+1)\tau), \end{aligned} \tag{A.5}$$

where $e^{-j\omega_c\tau}$ in the numerator has been absorbed by ϕ and $e^{-j\omega_c 2\tau}$ in the denominator by ψ in (A.4). Note that the factor of 2 will be absorbed later by the bandpass convolution operation.

Since the demodulation is performed coherently, it is assumed that the phase shift caused by ϕ can be ignored. Furthermore, it is assumed that the automatic gain controllers in the receiver makes $|\phi| = 1$. Consequently, $\phi = 1$ and is ignored in the model. In addition, it can be observed that the channel has a pure delay of τ, which we also ignore as it has no effect on the received signal. Therefore, the channel lowpass equivalent becomes after these assumptions

$$\tilde{h}(t) = 2\sum_{l=0}^{\infty}\psi^l\delta(t-2l\tau) \tag{A.6}$$

$$\tilde{H}(\omega) = \frac{2}{1-\psi e^{-j\omega 2\tau}}, \quad |\omega| < W. \tag{A.7}$$

Received Signal

The baseband representation of the received signal at the input of the equalizer after matched filtering consists of the baseband convolution of the transmitted signal with the equivalent channel, convolved with the matched filter plus the equivalent noise term also convolved with the matched filter, i.e.:

$$\tilde{r}(t) = \frac{1}{2}(\tilde{s} * \tilde{h} * p_{\text{MF}})(t) + (\tilde{n} * p_{\text{MF}})(t). \tag{A.8}$$

The factor $\frac{1}{2}$ comes from the equivalent lowpass convolution between $\tilde{s}(t)$ and $\tilde{h}(t)$. The convolution with $p_{\text{MF}}(t)$ does not require scaling since it is already lowpass.

Substituting (A.5) in (A.8) and using the sifting property of the $\delta(t)$ function, the received signal after the matched filter, is finally expressed as

$$\tilde{r}(t) = \sum_{k=-\infty}^{\infty} \sum_{l=0}^{\infty} \psi^l A_k g(t - kT - 2l\tau) + v(t) \tag{A.9}$$

where by definition $g(t) = (p * p_{\text{MF}})(t)$ (the time delay introduced by the matched filter is ignored because it has no consequences) and $v(t)$ is given by

$$v(t) = (\tilde{n} * p_{\text{MF}})(t) = \int_{-\infty}^{\infty} \tilde{n}(\xi) p_{\text{MF}}(t - \xi) d\xi. \tag{A.10}$$

The real and imaginary parts of $\tilde{r}(t)$ corresponds to the upper and lower branch respectively in Fig. 2.4 after the matched filters. The factors of two in the demodulator scale the signals so that the correspondences are exact.

Appendix B

Fourier Series Coefficients for the Mean of the Received Signal

In this Appendix, the Fourier series coefficients for the mean of the received signal, $u(t)$, $0 \leq t \leq T_{\text{o}}$ are derived. By definition, the Fourier series coefficients are given by

$$U(\omega_q) = \frac{1}{T_{\text{o}}} \int_0^{T_{\text{o}}} u(t) e^{-j\omega_q t} dt, \quad \omega_q = \frac{2\pi q}{T_{\text{o}}}, \quad q \in \mathbb{Z} \tag{B.1}$$

where T_{o} is the observation time. Recall from (3.15) that $u(t)$ is given by

$$\begin{aligned} u(t) &= \sum_{k=-\infty}^{\infty} \sum_{l=0}^{\infty} \psi^l A_k g(t - kT - 2l\tau - \epsilon) \\ &= \frac{1}{2} (\tilde{h} * \tilde{s} * p_{\text{MF}})(t - \epsilon), \end{aligned} \tag{B.2}$$

where $\tilde{h}(t)$ and $\tilde{s}(t)$ are the lowpass equivalent channel impulse response and transmitted signal respectively, as defined in Appendix A and $p_{\text{MF}}(t)$ is the matched filter. Using the inverse Fourier transform to replace the expressions for $\tilde{h}(t)$, $\tilde{s}(t)$ and $p_{\text{MF}}(t)$, (B.2) then becomes

$$u(t) = \sum_{k=-\infty}^{\infty} A_k \frac{1}{2\pi} \int_{-\infty}^{\infty} F(\omega) G(\omega) e^{-j\omega kT} e^{j\omega t} d\omega, \tag{B.3}$$

where $F(\omega) \equiv F(\omega;\boldsymbol{\theta})$ is the composite channel response, which depends on the parameter $\boldsymbol{\theta}$ and includes the synchronization offset effects. It is defined by

$$F(\omega;\boldsymbol{\theta}) = \frac{1}{2}\tilde{H}(\omega)e^{-j\omega\epsilon}, \tag{B.4}$$

where the channel lowpass equivalent frequency response $\tilde{H}(\omega)$ is defined in (A.7). Substituting the equation (B.3) for $u(t)$ in (B.1), the expression for the Fourier series coefficients now becomes

$$U(\omega_q) = \frac{1}{2\pi}\int_{-\infty}^{\infty} F(\omega)G(\omega)\sum_{k=-\infty}^{\infty} A_k e^{-j\omega kT}\underbrace{\frac{1}{T_\mathrm{o}}\int_0^{T_\mathrm{o}} e^{j(\omega-\omega_q)t}dt}_{Q(\omega-\omega_q)}\,d\omega. \tag{B.5}$$

Through simple integration, it can be shown that $Q(\omega-\omega_q)$ is given by

$$Q(\omega-\omega_q) = e^{j(\omega-\omega_q)\frac{T_\mathrm{o}}{2}}\,\frac{sin(\omega-\omega_q)\frac{T_\mathrm{o}}{2}}{(\omega-\omega_q)\frac{T_\mathrm{o}}{2}}. \tag{B.6}$$

The main lobe of $Q(\omega)$ (which has the form of a sinc function) in this case is inversely proportional to T_o. Therefore, if $T_\mathrm{o} \gg T$, i.e. N is large, then it can be assumed that $F(\omega)$ and $G(\omega)$ vary slowly within an interval of $\Delta\omega = \frac{2\pi}{T_\mathrm{o}}$. This assumption allows to extract $F(\omega)$ and $G(\omega)$ from the integral in (B.5). The expression for the Fourier series coefficients of $u(t)$ then becomes

$$U(\omega_q) \simeq F(\omega_q)G(\omega_q)\sum_{k=-\infty}^{\infty} A_k\frac{1}{2\pi}\int_{-\infty}^{\infty} e^{-j\omega kT}e^{j(\omega-\omega_q)\frac{T_\mathrm{o}}{2}}\,\frac{\sin((\omega-\omega_q)\frac{T_\mathrm{o}}{2})}{(\omega-\omega_q)\frac{T_\mathrm{o}}{2}}d\omega. \tag{B.7}$$

By using the change of variable $\omega' = \omega - \omega_q$, the previous equation simplifies to

$$U(\omega_q) \simeq F(\omega_q)G(\omega_q)\sum_{k=-\infty}^{\infty} A_k e^{-j\omega_q kT}\frac{1}{2\pi}\int_{-\infty}^{\infty}\frac{\sin(\frac{\omega' T_\mathrm{o}}{2})}{\frac{\omega' T_\mathrm{o}}{2}}e^{j(\frac{T_\mathrm{o}}{2}-kT)\omega'}d\omega'. \tag{B.8}$$

The integral in (B.7) is simply the inverse Fourier transform of a $\sin(x)/x$ type of function evaluated at time $t = T_\mathrm{o}/2 - kT$. It is given by

$$F^{-1}\left[\frac{\sin(\omega T_\mathrm{o}/2)}{\omega T_\mathrm{o}/2}\right]_{t=T_\mathrm{o}/2-kT} = \frac{1}{T_\mathrm{o}}\,\mathrm{rect}(\frac{T_\mathrm{o}/2-kT}{T_\mathrm{o}}), \tag{B.9}$$

where the rect function is defined as

$$\mathrm{rect}(t) = \begin{cases} 1, & |t| \leq \frac{1}{2} \\ 0, & \text{elsewhere}. \end{cases} \tag{B.10}$$

Therefore, using (B.9), the expression for the Fourier series coefficients now becomes

$$U(\omega_q) \simeq F(\omega_q)G(\omega_q) \sum_{k=-\infty}^{\infty} A_k e^{-j\omega_q kT} \frac{1}{T_\mathrm{o}} \mathrm{rect}(\frac{1}{2} - \frac{kT}{T_\mathrm{o}}). \tag{B.11}$$

If the observation interval corresponds to an integer number of symbol duration, i.e. $T_\mathrm{o} = NT$, then the rectangular function in (B.11) eliminates the symbols in the summation outside of the observation interval, reducing the sum over k to the range $0 \leq k < N$. Let $D(\omega)$ denote the contribution of the data, i.e.:

$$D(\omega) = \sum_{k=0}^{N-1} A_k e^{-j\omega kT}. \tag{B.12}$$

Then, the expression for the Fourier series coefficients of the mean of the received signal finally becomes

$$U(\omega_q) \simeq \frac{1}{T_\mathrm{o}} F(\omega_q; \boldsymbol{\theta}) G(\omega_q) D(\omega_q), \tag{B.13}$$

where the reference to the parameter $\boldsymbol{\theta}$ emphasizes the fact that only the composite channel frequency response $F(\omega; \boldsymbol{\theta})$ depends on the parameters in this expression.

References

[1] T. Shiba, A. Yuhara, K. Oda, and K. Tsubouchi, "Study of triple transit echo for time side-lobe of SAW matched filter," in *Ultrasonics Symposium, 1996. Proceedings, IEEE*, vol. 1, pp. 187–192, Nov. 1996.

[2] R. Pastore, J. Kosinski, and H. Cui, "An improved tunable filter topology for HF preselection," in *Frequency Control Symposium. Proceedings of the 1998 IEEE International*, pp. 575–579, May 1998.

[3] S. Qureshi, "Adaptive equalization," *Proceedings of the IEEE*, vol. 73, pp. 1349–1387, Sept. 1985.

[4] S. Koike, "Adaptive step size sign algorithm for application to adaptive filtering in digital qam communications," in *ICASSP, IEEE International Conference on Acoustics, Speech and Signal Processing - Proceedings*, vol. 6, pp. 3753–3756, 2001.

[5] L. Gay, Steven and S. Tavathia, "The fast affine projection algorithm," in *Acoustics, Speech, and Signal Processing, 1995. ICASSP-95., 1995 International Conference on*, vol. 5, pp. 3023 – 3026, May 1995.

[6] C.-H. Tseng and C.-B. Lin, "A frequency-domain approximate RLS algorithm for blind equalization of mobile communication channels," in *Personal, Indoor and Mobile Radio Communications, 1996. PIMRC'96., Seventh IEEE International Symposium on*, vol. 3, pp. 873–877, Oct. 1996.

[7] D. Godard, "Self-recovering equalization and carrier tracking in two-dimensional data communication systems," *IEEE Transactions on Communications*, vol. COM-28, pp. 1867–1875, Nov. 1980.

[8] C. Johnson, Jr., P. Schniter, T. Endres, J. Behm, D. Brown, and R. Casas, "Blind equalization using the constant modulus criterion: a review," *Proceedings of the IEEE*, vol. 86, pp. 1927–1950, Oct. 1998.

[9] H. Van Trees, *Detection, Estimation, and Modulation Theory, Part I*. John Wiley and Sons, Inc, 1968.

[10] A. Papoulis, *Probability, Random Variables, and Stochastic Processes*. McGraw-Hill, third ed., 1991.

[11] M. Davis and R. Vinter, *Stochastic Modelling and Control*. Monographs on Statistics and Applied Probability, Chapman and Hall, 1985.

[12] M. Wax and A. Lesh, "Joint estimation of time delays and directions of arrival of multiple reflections of a known signal," *IEEE Transactions on Signal Processing*, vol. 45, pp. 2477–2484, Oct. 1997.

[13] M. Wax and T. Kailath, "Optimum localization of multiple sources by passive arrays," *IEEE Transactions on Acoustics, Speech, and Signal Processing*, vol. ASSP-31, pp. 1210–1217, Oct. 1983.

[14] D. Cheng, *Field and Wave Electromagnetics*. Addison-Wesley, second ed., 1989.

[15] Storm Products Company, "Microwave Cable 421-012 Specifications." `"http://www.stormproducts.com/microwave"`.

[16] J. Proakis, *Digital Communications*. McGraw-Hill, third ed., 1995.

[17] S. Haykin, *Communication Systems*. John Wiley & Sons, Inc, third ed., 1994.

[18] A. Leon-Garcia, *Probability and Random Processes for Electrical Engineering*. Reading, Mass. : Addison-Wesley, 1994.

[19] R. Monzingo and T. Miller, *Introduction to Adaptive Arrays*. Wiley-Interscience, New York, 1980.

[20] D. Luenberger, *Linear and Nonlinear Programming*. Addison-Wesley, second ed., 1984.

[21] V. MacDonald and P. Schultheiss, "Optimum passive bearing estimation in a spatially incoherent noise environment," *The Journal of the Acoustical Society of America*, vol. 46, no. 1 (Part 1), pp. 37–43, 1969.

[22] W. Press, S. Teukolsky, W. Vetterling, and B. Flannery, *Numerical Recipes in C*. Cambridge University Press, second ed., 1992.

[23] The Mathworks, *Optimization Toolbox User's Guide*. 2001.

[24] S. Haykin, *Adaptive Filter Theory*. Prentice Hall, third ed., 1996.

[25] J. Proakis and D. Manolakis, *Digital Signal Processing, Principles, Algorithms and Applications*. Prentice Hall, third ed., 1996.

[26] A. Oppenheim, A. Willsky, and Nawab S. Hamid, *Signals & Systems*. Prentice-Hall, second ed., 1996.

[27] T. Laakso, V. Välimäki, M. Karjalainen, and U. Laine, "Splitting the unit delay," *IEEE Signal Processing Mag.*, vol. 13, pp. 30–60, Jan. 1996.

[28] D. Brandwood, "A complex gradient operator and its application in adaptive array theory," *IEEE Proceedings*, vol. 130, pp. 11–16, Feb. 1983.

[29] T. Parks and C. Burrus, *Digital Filter Design*. Topics in Digital Signal Processing, John Wiley & Sons, Inc., 1987.

[30] C. Farrow, "A continuously variable digital delay element," in *ISCAS, IEEE International Symposium on Circuits and Systems - Proceedings*, pp. 2641–2645, 1988.

[31] K. Scarbrough, N. Ahmed, and C. Carter, "On the simulation of a class of time delay estimation algorithms," *IEEE Transactions on Acoustics, Speech, and Signal Processing*, vol. ASSP-29, pp. 534–540, June 1981.